RECENT ADVANCES IN SURFACE TREATMENT AND ELECTRODEPOSITION

T.S.N. Sankara Narayanan[1,*] and S.K. Seshadri[2]

[1]*National Metallurgical Laboratory, Madras Centre, CSIR Complex Taramani, Chennai-600 113, India*
[2]*Department of Metallurgical and Materials Engineering Indian Institute of Technology Madras, Chennai-600 036, India*

ABSTRACT

Surface degradation processes such as wear, oxidation, corrosion and fatigue cause failure of many engineering components under varied circumstances. Among the various surface engineering processes, phosphate conversion coatings and, electro- and electroless plating processes have received widespread acceptance following their less complex processing sequence and cost-effectiveness. The present review addresses the recent developments in the areas of phosphate conversion coatings, electrodeposition and electroless deposition.

Key words: Surface treatment, phosphate conversion coating, electrodeposition, electroless deposition, composite coatings, duplex coating, graded coating, multilayer coating

1. INTRODUCTION

Surface degradation processes such as wear, oxidation, corrosion and fatigue cause failure of many engineering components under varied circumstances. This has led to the development of an interdisciplinary subject

* For correspondence
Tel: 91-44-22542077; Fax: 91-44-22541027
E-mail: tsnsn@rediffmail.com; tsnsn2005@yahoo.co.in

called as surface engineering in the early 1980's. Surface engineering can be defined as the design of a substrate and surface together as a system to produce a cost-effective performance enhancement of which neither is capable on its own. Although a variety of techniques, such as physical vapour deposition (PVD), chemical vapour deposition (CVD), etc., are available for engineering the surfaces to impart the desirable characteristics, phosphate conversion coatings and, electro- and electroless plating processes have received widespread acceptance following their less complex processing sequence and cost-effectiveness. The present review aims to address the recent developments in the areas of phosphate conversion coatings, electrodeposition and electroless deposition.

2. PHOSPHATE CONVERSION COATINGS

Phosphating is the most widely used metal pretreatment process for the surface treatment and finishing of ferrous and non-ferrous metals. Due to its economy, speed of operation and the ability to provide good corrosion resistance, wear resistance, adhesion and lubricative properties, it plays a significant role in the automobile, process and appliance industries /1/. The recent developments in phosphating include acceleration of low temperature phosphating process by galvanic coupling, cathodic and anodic electro-chemical treatments, manganese and calcium modified zinc phosphate coating for galvanized steel and development of polyphosphate coatings.

2.1 Acceleration of low temperature phosphating process

In recent years, low temperature phosphating process has assumed significance due to the escalating energy costs. It is a viable option to meet the energy demand, which is a major crisis in the present day scenario, and to eliminate the difficulties encountered due to scaling of heating coils and over heating of the bath. However, the rate of deposition of phosphate coating is very slow in this process and needs to be accelerated by some means. Acceleration of low-temperature phosphating process by utilizing the galvanic coupling methodology and by cathodic- and anodic electrochemical treatments and viability of these techniques for industrial applications has been explored by Sankara Narayanan and his co-workers /2-11/.

2.1.1 Acceleration of phosphating by galvanic coupling technique

This technique involves galvanic coupling of mild steel with metals (or alloys) that are nobler than it, as a means of accelerating low temperature phosphating process /2-5/. Being a conversion coating process, metal dissolution is the basis of phosphate coating formation. When the mild steel is galvanically coupled with metals (or alloys) that are nobler than it, the mild steel becomes the anode and the galvanic potential exerted by the couple determines the extent of metal dissolution and coating formation. Galvanic coupling accelerates the rate of metal dissolution, enables quicker consumption of free acid and earlier attainment of the point of incipient precipitation (PIP), which results in a higher coating weight compared to that obtained in uncoupled condition. The effect of galvanic coupling of mild steel with stainless steel, nickel, brass, copper and titanium, with a cathode to anode area ratio of 1:1, on the extent of iron dissolution and coating weight is given in Table 1.

Table 1

Effect of galvanic coupling of mild steel with different cathode materials with a cathode to anode area ratio of 1:1 on the extent of iron dissolution and the phosphate coating weight (adapted from /5/)

System studied	Iron dissolved during phosphating (g/m^2)	Coating weight (g/m^2)
Uncoupled mild steel	4.61	8.04
Mild steel coupled with stainless steel	5.05	8.75
Mild steel coupled with nickel	5.29	9.72
Mild steel coupled with brass	8.64	11.50
Mild steel coupled with copper	8.70	12.83
Mild steel coupled with titanium	9.50	17.50

The mechanism of phosphating of mild steel under galvanically coupled condition differs from the one in uncoupled condition. In galvanically coupled condition, both metal dissolution and coating formation occurs at the mild steel substrate and hydrogen evolution occurs at the cathode while in

uncoupled condition, all these reactions occur on the mild steel substrate itself. Increased rate of metal dissolution and increase in surface sites for coating deposition following the shift in hydrogen evolution reaction to the cathode enables the formation of a higher coating weight under galvanically coupled condition. The zinc phosphate coating obtained by galvanic coupling technique is uniform, consists of fine grained crystals, richer in phosphophyllite phase, possess better thermal and chemical stabilities and offer improved corrosion resistance compared to those obtained under uncoupled condition. The Nyquist plot of zinc phosphate coatings prepared under uncoupled and galvanically coupled conditions (area ratio: 1:1) in 3.5% NaCl solution is shown in Fig. 1. The extent of corrosion protection of phosphate coatings obtained using different galvanic couples and different area ratios is largely a function of coating weight obtained under such conditions. The study reveals that zinc phosphate coating with the desired coating thickness could be obtained by choosing the appropriate cathode materials, anode to cathode area ratios and processing time at low temperatures. The easy adaptability of this methodology even in existing processing stages makes it a very promising development. The formation of higher amount of the sludge is the major limitation of this methodology.

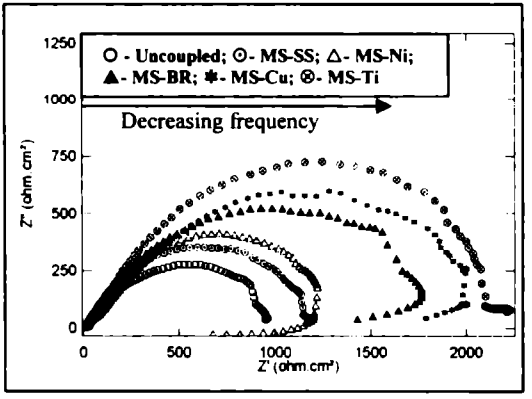

Fig. 1: Nyquist plot of zinc phosphate coatings prepared under uncoupled and galvanically coupled condition (area ratio = 1: 1) in 3.5% NaCl solution at their respective open circuit potentials (adapted from /5/)

2.1.2 Cathodic electrochemical treatment process

Cathodic electrochemical treatment involves the application of a cathodic current to the mild steel substrate immersed in the phosphating bath, similar

to that of electrodeposition process /6-9/. This treatment enables the formation of a zinc-zinc phosphate composite coating on mild steel. The coating formation proceeds through three stages: deposition of zinc, deposition of zinc phosphate and codeposition of zinc and zinc phosphate, respectively, are the predominant reactions in these three stages. The mechanism of coating formation in this process involves mainly proton reduction (hydrogen evolution) and the associated counter-phenomenon viz., zinc deposition, in the first stage followed by the predominant zinc phosphate deposition in the second stage. The competition between deposition of zinc and zinc phosphate continues until an equilibrium is established, after which they proceed with almost equal rates. The type of coating obtained by cathodic electrochemical treatment process is a zinc–zinc phosphate composite coating compared to zinc and iron phosphate coating obtained by conventional chemical treatment process. The zinc–zinc phosphate composite coatings exhibit excellent stability in 3.5% sodium chloride solution; they last for a week with no red rust formation. The composite layer of zinc and zinc phosphate provides both sacrificial and barrier layer protection and significantly increases the corrosion resistance. In phosphated and painted samples subjected to salt spray testing, a white corrosion product, as a result of preferential dissolution of metallic zinc, is observed in the scribed region for samples phosphated by cathodic treatment as opposed to the red rust in case of unphosphated and painted mild steel (Fig. 2).

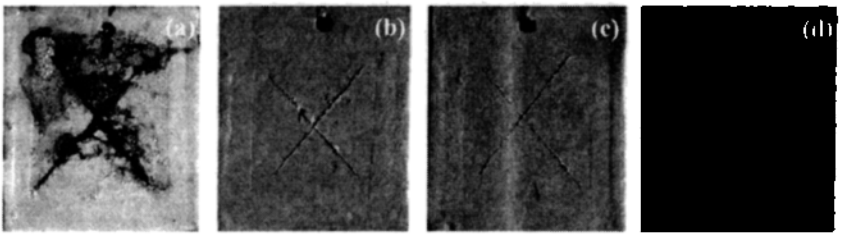

Fig. 2: Performance of phosphated and painted mild steel substrates after 96 hours of salt spray test (a) unphosphated mild steel; (b–d) mild steel phosphated using cathodic electrochemical treatment at (b) 4 mA/cm^2; (c) 5 mA/cm^2; (d) 6 mA/cm^2 (Reprinted from *Electrochimica Acta*, Vol. 51(2), S. Jegannathan, T.S.N. Sankara Narayanan, K. Ravichandran and S. Rajeswari, Performance of zinc phosphate coatings obtained by cathodic electrochemical treatment in accelerated corrosion tests, pp. 247-256 (2005) with permission from Elsevier Science)

2.1.3 Anodic electrochemical treatment process

Anodic electrochemical treatment involves the application of an anodic current to the mild steel substrate immersed in the phosphating bath /9-11/. This treatment is similar to the galvanic coupling method in which the mild steel is made as the anode during phosphate coating formation. The coating formation proceeds through two stages: metal dissolution and deposition of phosphate coating are the predominant reactions during the first and second stages, respectively. The onset of phosphate coating occurs following the initial metal dissolution, displacement of protons away from the interface and attainment of the PIP. Further to this, both metal dissolution and coating formation continue throughout the entire duration of deposition. The mechanistic aspects associated with the anodic phosphating resemble those of the conventional phosphating process but with accelerated metal dissolution. For depositing phosphate coating with a weight of 10 g/m^2, it will take about 50 minutes by chemical deposition, whereas by using the same bath composition with anodic treatment, the processing time could be reduced to 30 minutes; a degree of acceleration of 40%. However, compared to conventional chemical treatment process, the conversion ratio (ratio of coating weight to iron dissolved) is very low in the anodic treatment process. Anodic electrochemical treatment leads to the formation of needle-like crystals, which is characteristic of the phosphophyllite phase ($Zn_2Fe(PO_4)_2 \cdot 4H_2O$) (Fig. 3).

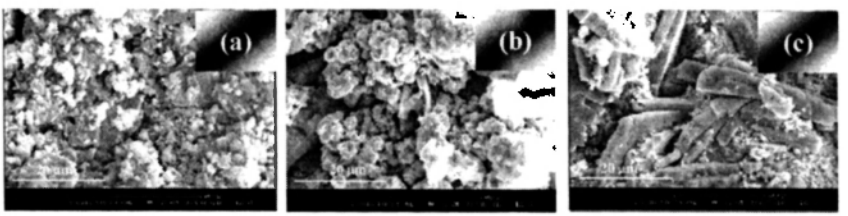

Fig. 3: Surface morphology of the phosphate coatings obtained by anodic electrochemical treatment at different current densities (a) 4 mA/cm^2; (b) 5 mA/cm^2; and (c) 6 mA/cm^2 (Reprinted from *Progress in Organic Coatings,* Vol. 57, T.S.N. Sankara Narayanan, S. Jegannathan, K. Ravichandran and S. Rajeswari, Evaluation of the corrosion resistance of phosphate coatings obtained by anodic electrochemical treatment, pp. 392-399 (2006) with permission from Elsevier Science)

The refinement of crystals is due to the continuous dissolution and re-precipitation of the phosphate coating by the phosphoric acid formed during the anodic treatment. The coatings obtained by the anodic phosphating process are rich in the phosphophyllite phase with a smaller proportion of hopeite phase and iron phosphate. The porosity of the anodically phosphated mild steel substrate is relatively higher than that of conventionally phosphated ones. Phosphate coatings obtained by anodic treatment primarily act as a barrier layer, similar to the coatings obtained by chemical treatment, to prevent the ingress of corrosive media. Since phosphate coatings obtained by anodic treatment process are more porous, they will suit most for applications that require higher oil-retaining capacity.

The deposition of zinc phosphate coatings on mild steel by cathodic and anodic electrochemical treatments has several advantages and limitations/12/. A comparison of the salient features of the cathodic and anodic treatment processes is given in Table 2.

2.2 Manganese and calcium modified zinc phosphate coating

Palraj *et al.* /13/ have evaluated the performance of phosphate coatings on galvanized steel (GS) obtained using calcium- and manganese- modified zinc phosphating baths and compared with those obtained from unmodified zinc phosphating baths, in terms of adhesion of epoxy coating and corrosion resistance. The unmodified zinc phosphate coating on GS surface due to its less porous nature, exhibits cohesive failure of the matrix. Manganese modified phosphate coating enhances the adhesion due to its more porous nature and galvanic action on the GS matrix compared to the unmodified and calcium modified zinc phosphate coating. Surface pretreatment with manganese modified phosphate coating on GS surface is more effective than the calcium modified and zinc phosphate system as far as corrosion protection is concerned.

Table 2

Comparison of cathodic and anodic electrochemical treatment processes (adapted from /9, 12/)

Parameter	Cathodic treatment	Anodic treatment
Bath constituents	Essential constituents – ZnO, H_3PO_4 and NaOH	Essential constituents – ZnO, H_3PO_4, NaOH and $NaNO_2$
Special additive	No special additives	No special additives
Requirement of accelerator	No accelerator is necessary	Accelerator addition is essential to prevent polarization of the cathode
Energy requirement	Capable of producing good quality coatings even at low temperature	Capable of producing good quality coatings even at low temperature
Eco-friendliness	More eco-friendly	Less eco-friendly
Operational problems	Disintegration of graphite cathode - Use of anode bag is essential to get good quality deposits. Being a cathodic process, it might induce hydrogen embrittlement - desirable to adopt a post-baking operation to relive the hydrogen	Deposition of metallic zinc at the graphite cathode
Iron dissolution	No iron dissolution	Heavy iron dissolution
Coating weight	High; Permits to build the desired coating weight by increasing the time	Medium; Similar to conventional phosphating
Sludge formation	No sludge formation	Heavy sludge formation

Table 2 (continued)

Reactions at Mild steel	Deposition of zinc and phosphate; H_2 evolution;	Iron dissolution; Phosphate deposition
Means of attainment of PIP	Proton consumption for H_2 evolution reaction	Drifting of protons away from the electrode vicinity
Coating composition	Zinc phosphate (hopeite phase); Metallic zinc	Zinc-iron phosphate (phosphophyllite) Zinc phosphate (hopeite) Iron phosphate
Colour and appearance	Grey with bright crystalline luster	Greyish white with no metallic luster
Uniformity of the coating	Uniform	Uniform
Adhesion	Good	Good
Porosity	Very low porosity	More porous than conventional phosphating process
Thermal stability	Comparable with anodic and conventional phosphating processes	Comparable with cathodic and conventional phosphating processes
Parameter	Cathodic treatment	Anodic treatment
Chemical stability	Relatively lower than conventional and anodic phosphating processes	Relatively higher than cathodic phosphating process; Resembles that of conventional phosphating process

Table 2 (continued)

Surface morphology	Plate/flower-like crystals	Needle-like crystals
Immersion test	No red rust formation after 12 hours of immersion; Solution remains colourless	No red rust formation after 12 hours of immersion; Solution remains colourless
	Weight loss after 24 hours is considerably lower than conventional and anodic phosphating process	Weight loss after 24 hours is lower than conventional phosphating; relatively higher than cathodic phosphating
	Formation of zinc based corrosion products (white rust) which resist further corrosion	Formation of red rust leading to further corrosion
Salt spray test	Prevents spreading of corrosion from the scribe	Prevents spreading of corrosion from the scribe
	White rust formation at the scribe	Red rust formation at the scribe
Potentiodynamic Polarization studies	Greater shift in E_{corr} values towards cathodic values compared to uncoated mild steel (-1000 to -1100 mV vs. SCE)	A slight shift in E_{corr} values towards anodic values compared to uncoated mild steel (-680 to -700 mV vs. SCE)
	With increase in immersion time the E_{corr} values shift towards more anodic values	Behaves like conventionally phosphated mild steel

Table 2 (continued)

Electrochemical impedance studies	Nyquist plot exhibits a small semicircle and an inductive loop in the initial period	Nyquist plot exhibits a semicircle and a diffusion tail; Semi-infinite and finite length diffusion behaviour
	Improvement of corrosion resistance with time	Behaves like conventionally phosphated mild steel
Galvanic corrosion	Protects the uncoated mild steel substrate during the initial periods of immersion	Accelerates the corrosion of uncoated mild steel during the initial periods of immersion
	With increase in time, the corrosion of uncoated steel is accelerated	With increase in time, the corrosion of uncoated steel will proceed further
Cathodic delamination	Mean delamination distance is less than 1 mm	Mean delamination distance is less than 1 mm
Corrosion of phosphated and painted steel	Prevents the corrosion of the base metal for a long time. R_{ct} values are in the range of 10^5 Ohms.cm^2	Prevents the corrosion of the base metal for a reasonable time. R_{ct} values are in the range of 10^4 to 10^5 Ohms.cm^2

2.3 Polyphosphate coating for corrosion protection of steel sheets

Rust preventive oils (RPO) have been used as a temporary corrosion protection measure of steel sheets against atmospheric corrosion during storage and transit. A thin film of RPO is usually applied for this purpose. However, when the storage conditions exceed 2 to 3 months, the protection offered by the thin film of RPO becomes ineffective. Use of thicker films, though effective to some extent would cause problems during the further processing stages. Consumption of alkali degreasing chemicals for the removal of excess oil from the steel sheets is one of the commonly encountered problems. Treatment of steel sheets with RPO is considered to be non-compatible with the surface pretreatment lines in automobile and white good industries.

Rout *et al.* /14/ have considered polyphosphate coating as an alternative for the RPO treatment. The polyphosphate coating formulation developed by them is a mixture of 80% hydroxy ethyl di-phosphonic acid (48 to 50% v/v) stabilized by the addition of 20% phosphoric acid (4 to 8% v/v). The solution also contains rust inhibiting agents, surface active agents, ethylene glycol as an extender, N, N-dimethyl amine along with tri ethanol amine as a neutralizer cum corrosion inhibitor and silicone oil as a leveling agent. The polyphosphate coating is applied by a roll coater, followed by squeeze rolling and drying at 40 °C. The polyphosphate coated steel offers better corrosion resistance compared to steel surfaces treated with rust preventive oil (RPO) and conventional phosphate coating in 3.5% NaCl solution. The excellent corrosion resistance offered by polyphosphate coating is due to its ability to chemically adhere to metal surface through Fe–P bonding. The strong bonding between the metal surface and the polyphosphate coating delays the diffusion of water/ions to the substrate whereas in case of steel surfaces treated with RPO and conventional phosphate coating, the diffusion of water/ion is very prominent as there is no chemical bond exists between the steel and the coating interface.

2.4 Polymanganese phosphate coating on galvannealed steel

Galvannealed (GA) steel sheets are used for automobile components due of its excellent corrosion resistance, good paintability and weldability. A galvannealed coating weight of 50 g/m^2/side (coating thickness ~ 7 μm) is considered to be necessary for providing 10 years perforation corrosion

resistance and 5 years cosmetic corrosion resistance. However, increase in coating weight of GA causes press formability problem because of flaking of coating (powdering). The flakes thus formed stick to the die face, which warrants frequent cleaning of die and affects its precision. The press formability problems can be significantly reduced by giving a post-treatment coating which avoids direct contact between the GA coatings and the dies. Rout *et al.* /15/ have explored the possibility of using polymanganese phosphate as a post-treatment coating on galvannealed steel sheets. The performance of the polymanganese phosphate coating is evaluated in terms of reduction in coefficient of friction and powdering characteristics compared to untreated galvannealed steel.

The polymanganese phosphate coating is applied on galvannealed steel sheets by immersion treatment at 40 °C for about 2 seconds followed by squeezing and room temperature drying. The polymanganese phosphate coating is uniform and dense with a crystallite size of 1 to 2 μm. The coating weight is of the order of 1.1 g/m^2. The coating primarily consists of rockbridgeite $\{Fe_5(PO_4)_3(OH)_5\}$ and manganese phosphate hydrate $\{Mn_2(P_2O_{12}).10H_2O\}$. The polymanganese phosphate coated galvannealed (GA) steel sheets with 1000 g/m^2 oil reduces the coefficient of friction with the die surface from 0.22 (in case of untreated GA surface) to 0.11 (in case of treated GA surface) indicating superior lubricating property. The granular nature of the phosphate coating acts as a lubricating base and helps to reduce the coefficient of friction. The manganese phosphate acts as an anti-sticking base and provides a smooth surface during forming operation. For polymanganese phosphate treated galvannealed steel sheet the amount of Fe powder generated during forming operation is about 5.9 mg whereas 12 mg of Fe powder is generated for untreated galvannealed steel sheet under similar conditions.

3. ELECTRODEPOSITION

The recent developments in electrodeposition include development of nanocrystalline nickel and nickel based alloy coatings, electrodeposited nanorods, multilayer, graded coatings and composite coatings. Nanocrystalline materials are of great industrial importance due to their improved properties especially chemical and mechanical properties. These materials are used as bulk as well as coatings to engineer the substrate surface. Electrodeposition is a versatile technique for producing

nanocrystalline materials. Metallic multilayer and graded coatings are emerging areas of research, which offer the possibility to manipulate the desirable characteristics so as to meet the demands of specific industrial applications. Electrodeposition is a relatively simple and cost-effective technique to prepare multilayer and graded coatings.

3.1 Electrodeposition of nanocrystalline nickel and nickel based alloy coatings

3.1.1 Nanocrystalline nickel coatings

Mishra and Balasubramaniam /16/ and Mishra *et al.* /17/ have prepared nanocrystalline nickel coatings with varying grain sizes in the range of 8–28 nm by direct and pulsed current electrodeposition technique using Watt's bath containing saccharine as the additive and evaluated their corrosion and tribological behaviour. The nanocrystalline Ni coatings are compressively strained and the extent of microstrain increases with a decrease in grain size. The microhardness of nanocrystalline nickel coating is found to increase when the grain size of nickel is decreased from 28 to 8 nm in accordance with the Hall–Petch relation. The increase in hardness is also reflected in the wear resistance of the nanocrystalline nickel coatings. The steady state coefficient of friction (COF) of polycrystalline nickel coatings with a grain size of 61 μm is around 0.62 whereas for nanocrystalline nickel coatings, the COF is almost half of that of polycrystalline nickel coatings. Among the nanocrystalline nickel coatings, reduction in grain size of nickel from 28 to 8 nm enables a decrease in COF from 0.55 to 0.16.

The corrosion behaviour of coarse-grained polycrystalline and nanocrystalline nickel coatings with different grain sizes was evaluated in 1 M H_2SO_4. The active–passive behavior in 1 M H_2SO_4 is exhibited by both nanocrystalline as well as conventional coarse-grained polycrystalline nickel coatings. The shift of zero current potential in the noble direction with decreasing grain size has been related to modification in cathodic reaction (hydrogen reduction) processes. The passive current density of nanocrystalline nickel coatings is higher than that of coarse-grained polycrystalline nickel coatings and confirms the defective nature of passive film formed on nanocrystalline nickel coatings. However, the tendency for localized corrosion is lower for nanocrystalline nickel coatings as indicated by the increased breakdown potential compared to the coarse-grained

polycrystalline nickel coatings. A systematic increase in the breakdown potential (E_b) with decrease in grain size of nanocrystalline nickel coatings is observed. The absence of any significant difference in the microstructural features of the nanocrystalline nickel coatings before and after polarization suggests that the breakdown in passivity is not localized but spread out over the whole surface. The corrosion rate of freshly exposed surfaces of nickel is found to decrease with the grain size, thereby indicating a greater hindrance to anodic dissolution by nanocrystalline nickel coatings.

3.1.2 Nanocrystalline nickel coating under the influence of an applied magnetic field

The deposition of a metal or an alloy by electric current in the presence of an applied magnetic field is known as magnetoelectrolysis (ME) or magneto electrolytic deposition. Ganesh *et al.* /18/ have studied the electrodeposition of nickel from a nickel sulphamate bath in the presence of a magnetic field applied at an angle of 45° to the cathode surface. A significant lowering of overpotential with time and a large negative shift in electrode potential are observed in the presence of a magnetic field. The magnetic field induced convection increases the mass transfer rate, reduces the concentration polarization and leads to the growth of fine grained deposits. The smallest grains are about 17 to 25 nm in size. The large shift in electrode potential on the application of magnetic field is attributed to the field-induced shift in chemical potential of the ferromagnetic nickel electrode. The study reveals that magnetic field-induced convective mass transfer enables the formation of a fine grain deposit of nickel as opposed to a layer type growth in its absence.

3.1.3 Nanocrystalline Ni-B alloy coatings

Electrodeposition of Ni-B alloy coating on mild steel using a dimethylamine borane (DMAB) modified Watt's bath and evaluation of its characteristic properties has been reported by Krishnaveni *et al.* /19-22/. Alloying of boron with nickel occurs due to the adsorption of DMAB on the already formed nickel surface and its subsequent decomposition to elementary boron. The extent of alloying of boron is determined by the distribution of DMAB and, the thickness of the diffusion layer at the cathode surface, regardless of the electrode potential. The boron content of the ED Ni-B alloy coating is determined by the ratio of rate of reduction of nickel and rate of decomposition of DMAB. An increase in this ratio with increase in current

density leads to a decrease in boron content of the ED Ni-B coating. The plating rate of ED Ni-B coating at 1 A/dm^2 is 12 μm/hour. The Ni-B coating electrodeposited at 1 A/dm^2 contains 97 wt.% nickel and 3 wt.% boron.

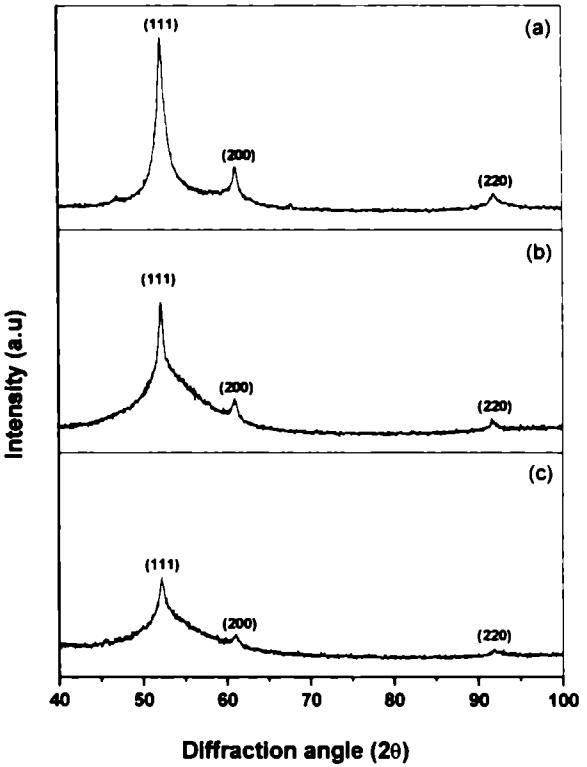

Fig. 4: X-ray diffraction pattern of Ni–B coatings electrodeposited at different current densities in their as-plated condition: (a) 0.4 A/dm^2; (b) 1 A/dm^2; and (c) 4 A/dm^2 (Reprinted from *Materials Chemistry and Physics* Vol. 99, K. Krishnaveni, T.S.N. Sankara Narayanan and S.K. Seshadri, Electrodeposited Ni-B coatings: Formation and evaluation of hardness and wear resistance, pp. 300- 308 (2006) with permission from Elsevier Science).

The microhardness of as-plated ED Ni–B coating is of the order of 609 ± 15 $HV_{0.1}$, which is considerably high compared to that of bulk Ni (100-150 $HV_{0.1}$) and ED Ni (250-350 $HV_{0.1}$). The hardness increases to 817 ± 20 $HV_{0.1}$ when the coating is heat-treated at 400 °C for 1 hour. At temperatures above 400 °C, the ED Ni-B coating begins to soften as a

result of coarsening of the Ni_3B particles, which thereby reduces the number of hardening sites. The wear resistance is higher for heat-treated ED Ni-B coatings compared to those obtained in as-plated condition. Heat-treatment enables the formation of hard Ni_3B phase, which has a low mutual solubility with iron resulting in an incompatible surface with the steel counterface, thereby increasing the wear resistance. The mechanism of wear in ED Ni-B coatings is intensive plastic deformation of the coating due to the ploughing action of the hard counter disk. The nanocrystalline nature and presence of cracks are primarily responsible for the observed corrosion behaviour of the ED Ni-B coating in their as-plated condition. Heat-treatment induces crystallinity of the ED Ni-B coating, which in turn increases the grain boundaries which are the active sites for corrosion attack. The cracks in the ED Ni-B coatings enable the electrolyte to penetrate through them.

3.1.4 Nanocrystalline Ni-W and Ni-Fe-W alloy coatings

Ni–W based alloys are known to exhibit higher hardness, higher heat resistance and better corrosion resistance compared to pure Ni. Ni-W based alloy coatings has been considered as an ecological alternative for chromium plating /23/. Sriraman *et al.* /24/ have studied the formation of nanocrystalline Ni-W alloy coatings by electrodeposition using an alkaline sodium citrate based bath and evaluated their hardness, crystallite size and wear resistance. The influence of current density and temperature on the tungsten content and crystallite size of Ni–W alloy deposits is studied. Increase in current density (from 0.05 to 0.20 A/cm^2) and bath temperature (from 75 to 85 °C) results in an increase in tungsten content of the coating leading to a reduction in crystallite size (Fig. 5). ED Ni–W alloy deposits prepared at 75 °C followed direct Hall–Petch relation, i.e., the hardness of the deposit increases with a reduction in the crystallite size. However, Ni–W alloy deposits prepared at 85 °C obey the direct Hall–Petch relation only above a critical crystallite size of 15 nm and follow inverse Hall–Petch relation below this critical size. The Ni–W alloy deposit with 9.33 at.% W prepared at 75 °C exhibits the maximum hardness of 638 HV. Wear resistance of Ni-W alloy deposits prepared at 75 °C increases due to the increase in hardness with a reduction in the crystallite size up to 20 nm. However, when the crystallite size is below 20 nm, brittle fracture of the coating due to extensive resistance to plastic deformation decreases the wear resistance. Wear resistance of Ni-W alloy deposits prepared at 85 °C

increases with a reduction in the crystallite size in the direct Hall–Petch region and decreases in the inverse Hall–Petch region. Ni–W alloy deposit with 6–8 at.% W exhibits superior wear resistance.

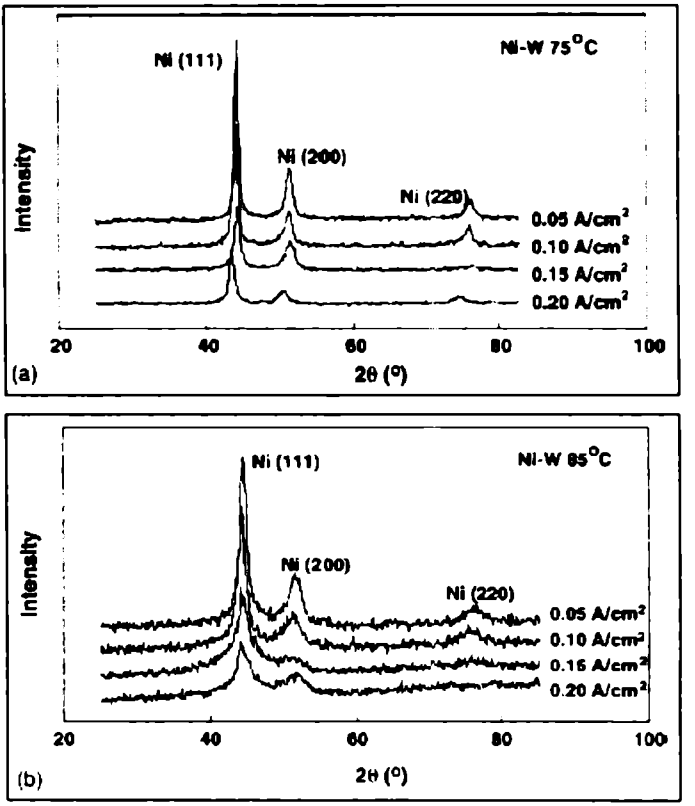

Fig. 5: XRD pattern of nanocrystalline Ni–W alloy coatings electrodeposited at different current densities and at temperatures (a) 75 °C; (b) 85 °C (Reprinted from *Materials Science and Engineering A,* Vol. 418, K.R. Sriraman, S. Ganesh Sundara Raman and S.K. Seshadri, Synthesis and evaluation of hardness and sliding wear resistance of electrodeposited nanocrystalline Ni–W alloys, pp. 303–311 (2006) with permission from Elsevier Science)

The electrodeposition of Ni-W alloy coatings was also studied by Eliaz *et al.* /25/, Sridhar *et al.* /26/ and Eliaz and Gileadi /27, 28/. The effect of bath chemistry, additives and operating conditions on the chemical

composition, microstructure and properties of Ni-W alloy coatings obtained from citrate-containing baths was studied by these authors. Eliaz *et al.*/ 25/ have suggested that the tungsten content in the ED Ni-W alloy coating could be increased either by increasing the concentration of citrate ions at low current density or by decreasing the concentration of citrate ions at high current density. Eliaz and Gileadi /27, 28/ have suggested that the induced codeposition of Ni-W alloy coatings results from the formation of a mixed ternary complex such as $[(Ni)(HWO_4)(Cit)]^{2-}$, which serves as the precursor for the deposition of the alloy. Sridhar *et al.* /26/ have studied the formation of Ni-W alloy coating from a bath containing nickel sulphate, sodium tungstate and tri-sodium citrate as a function of current density and temperature. It is evident from their work that plating conditions employed largely influence the structure of the ED Ni-W alloy coatings. At sufficiently high citrate concentrations, an amorphous Ni-W phase is formed at room temperature and different current densities whereas at elevated temperatures (50-70 °C) and low current density, formation of body-centered tetragonal Ni_4W phase is observed. The repeated formation of Ni_4W phase in ED Ni-W alloy coatings has been observed by Sridhar *et al.* /26/ for the first time.

Sriraman *et al.* /29, 30/ have also studied the formation of nanocrystalline Ni-Fe-W alloy coatings by electrodeposition using an alkaline sodium citrate based bath and evaluated their hardness, crystallite size, wear resistance and corrosion resistance. Increase in current density (from 0.05 to 0.20 A/cm^2) has resulted in an increase in iron and tungsten content of the deposit and leads to a reduction in crystallite size. Ni–Fe–W alloy coatings with 23 at.% Fe and 1.3 at.% W prepared at 0.1 A cm^2 exhibited the maximum hardness of 563 $HV_{0.1}$. The Ni-Fe-W alloy coatings followed direct Hall–Petch relation above a critical crystallite size of 12 nm and inverse Hall–Petch relation below that. With a reduction in the crystallite size, wear resistance increased in the direct Hall–Petch region and decreased in the inverse Hall–Petch region. Ni–Fe–W alloy coatings with 23 at.% Fe and 1.3 at.% W plated at 0.1 A cm^2 exhibited superior wear resistance.

Sriraman *et al.* /30/ have studied the corrosion behaviour of electrodeposited nanocrystalline Ni–W binary and Ni–Fe–W ternary alloy coatings in 3.5% NaCl and 1N H_2SO_4. The corrosion resistance of Ni–W alloys increased with tungsten content up to 7.54 at.% and then decreased. In case of Ni–Fe–W alloys it increased with tungsten content up to 9.20 at.% and then decreased. The ternary alloy coatings exhibit poor corrosion

resistance compared to binary alloy coating due to preferential dissolution of iron from the matrix. The superior corrosion resistance of Ni–W alloy films was due to preferential dissolution of nickel and formation of tungsten rich film on the surface, which inhibited further corrosion. Regardless of composition all the alloys exhibited passivation behaviour in 1N H_2SO_4 over a wide range of potentials due to the formation of tungsten rich film on the surface.

3.1.5 Nanocrystalline Cu-Ni alloy coatings

Recently, there has been a renewed interest in electrodeposited nanocrystalline Ni–Cu alloy and Ni/Cu multilayer coatings as they show giant magnetoresistance (GMR) properties and find application in magnetoresistive devices. Baskaran /31/ and Baskaran *et al.* /32/ have studied the formation of nanocrystalline Cu–Ni alloy films by PED using sodium citrate-based plating bath and evaluated their structural, morphology, thermal and magnetic properties. The Cu–Ni alloy films obtained at 2.5, 5, 7.5, 10, 15 and 20 A/dm^2 have a stoichiometry of $Cu_{0.98}Ni_{0.02}$, $Cu_{0.95}Ni_{0.05}$, $Cu_{0.89}Ni_{0.11}$, $Cu_{0.77}Ni_{0.23}$, $Cu_{0.56}Ni_{0.44}$ and $Cu_{0.38}Ni_{0.62}$, respectively, and they possess f.c.c. structure. The lattice constant decreases with increase in nickel content of the Cu–Ni alloy films (Fig. 6). The crystallite size lies in the range of 15 to 46 nm for as-plated alloy deposits and it increases from 20 to 114 nm, following vacuum annealing at 400 °C for 1 hour. The Cu–Ni alloy films obtained at 2.5 and 5.0 A/dm^2 are diamagnetic, the one obtained at 7.5 A/dm^2 exhibits a weak ferromagnetic activity, whereas those obtained at 10, 15 and 20 A/dm^2 are ferromagnetic. The saturation magnetization increases with increase in nickel content of the Cu–Ni alloy film.

Ghosh *et al.* /33/ have prepared dense nanocrystalline Cu-Ni alloy deposits with an average grain size of 2 to 30 nm by direct current (DC) and pulse current electrodeposition (PED) techniques and compared the corrosion behaviour of electrodeposited nanocrystalline Cu-Ni alloy having a similar composition with Monel-400 alloy in 3.0 wt.% NaCl. The corroded surface morphology of nanocrystalline Cu-Ni alloy deposits exhibits numerous overlapping of shallow pits akin to general type corrosion compared to the pitting type corrosion morphology observed for Monel-400 alloy. ED nanocrystalline Cu-Ni alloy deposit offers better resistance to pitting corrosion compared to the Monel-400 alloy.

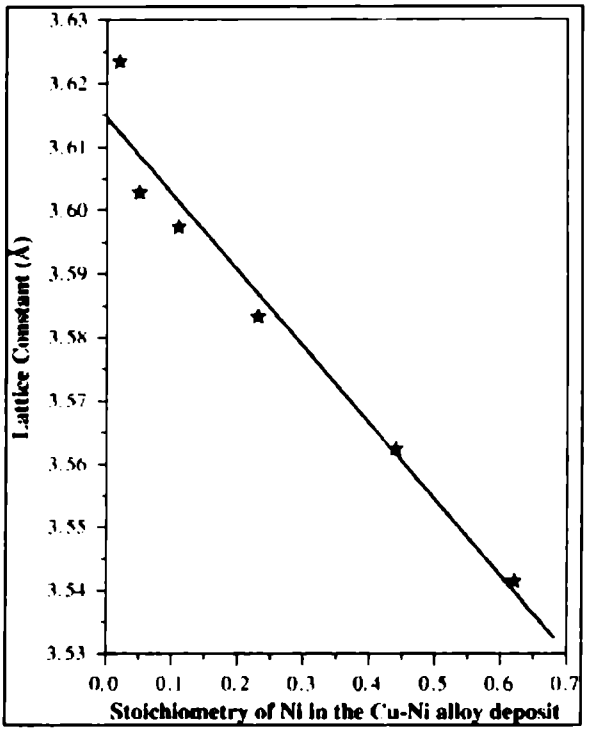

Fig. 6: Plot of the lattice constant of the Cu-Ni alloy films as a function of their composition (Reprinted from *Materials Letters,* Vol. 60(16), I. Baskaran, T.S.N. Sankara Narayanan and A. Stephen, Pulsed electrodeposition of nanocrystalline Cu–Ni alloy films and evaluation of their characteristic properties, pp. 1990-1995 (2006) with permission from Elsevier Science)

3.2 Electrodeposition of CoNiFe nanorods using AAO template

Magnetic nanowires are scientifically interesting and have potential applications in many areas of advanced nanotechnology, including patterned magnetic recording media, materials for optical and microwave applications, electroluminescent display devices and biological applications. For most of these applications, it is desirable to fabricate ultrafine nanostructures as well as arrays of such nanostructures over macroscopic areas. Ordered arrays of magnetic nanowires are particularly interesting to study, as it is possible to probe both the individual and collective behavior of the elements in a well-

defined and reproducible fashion. PED of CoNiFe alloy nanorods using porous anodized aluminum oxide (AAO) membrane (250 nm diameter) is explored by Baskaran /31/ using the following conditions: current density: 5 mA/cm^2; T_{on}= 1 ms; T_{off} = 0.9 ms; duty cycle = 10%; frequency = 1000 Hz. After deposition, the AAO membrane is selectively etched without damaging the CoNiFe alloy nanorods. The CoNiFe alloy nanorods are continuous and roughly parallel to one another. All of them have smooth surfaces with uniform diameters of about 200 nm, which is slightly less than the pore size of the template (250 nm diameter AAO membrane) used. These CoNiFe alloy nanorods will find application in the area of magnetic storage devices.

3.3 Electrodeposited multilayer coatings

3.3.1 Ni-B multilayer coatings

Krishnaveni /22/ has explored the possibilities of preparing Ni-B multilayer coatings by electrodeposition technique using (DMAB) modified Watts' bath, with DMAB as the source of boron. The Ni-B coatings electrodeposited at 0.4 A/dm^2 have a boron content of 3 wt.% whereas the boron content of the coating is considerably reduced when the current density is increased to 4 A/dm^2. The properties of the ED Ni-B coating, such as hardness, wear resistance, corrosion resistance, etc. is also found to vary significantly following the variation in the boron content of the coating as a function of current density. This suggests that ED Ni-B multilayer coatings having alternate layers of Ni-high B and Ni-low B could be prepared from a single bath by alternatively varying the current density between 0.4 and 4 A/dm^2. The Ni-B multilayer coating with a periodicity of 10 microns is prepared by alternatively varying the current density between 0.4 and 4 A/dm^2 for 90 and 14 minutes, respectively. It is essential to give an anodic etching at 0.2 A/dm^2 after electrodeposition of each individual layer to improve the quality as well as the uniformity of the coating. ED Ni-B multilayer coating is uniform and the compatibility between the layers is good. The microhardness of the Ni-B multilayer coating at every 10 micron thickness indicate a variation in the hardness, which is of the order of 654 $HV_{0.1}$ at the 10 μm thick layer prepared at 0.4 A/dm^2 and 340 $HV_{0.1}$ for the 10 μm thick layer prepared at 4 A/dm^2, due to the variation in the boron content in these layers. The ED Ni-B multilayer coatings prepared by alternatively varying the current density between 0.4 and 4 A/dm^2 suggest

that it is possible to manipulate the ED Ni-B multilayer coatings with the desirable characteristics, by suitably modifying the bath composition and/or operating conditions.

3.3.2 Cu-Ni multilayer coatings

Electrodeposition of Ni/Cu multilayer coatings with varying Ni sublayer thickness (t_{Ni}) ranging 1.8 to 11 nm, keeping the Cu sublayer thickness (t_{Cu}) fixed at 1.97 nm from sulphate based electrolyte has been carried out by Ghosh *et al.* /34/. XRD analysis confirmed the formation of homogeneous and compact multilayer structure. The hardness of the multilayers is found to be dependent on wavelength of the modulation. The stress level within the multilayer coatings decreases with increase in t_{Ni}. The order of wear rates for multilayer coatings is found to follow as the order of their (H/E) ratio and hardness. Among the multilayer coatings, coatings with a t_{Ni} of 7.2 nm has shown the lowest wear rate owing to its high (H/E) ratio, high hardness and low residual stress. The multilayer coating with very high and low t_{Ni} exhibits poor wear behaviour due to the very weak multilayer effect.

3.3.3 Compositionally modulated Zn-Co multilayer coatings

Electrodeposition of compositionally modulated Zn-Co multilayer coatings from acid chloride baths by single-bath technique and their corrosion behaviour was reported by Thangaraj *et al.* /35/. The corrosion resistance of the Zn-Co CMA coatings is higher than that of the monolithic Zn-Co coating with the same thickness. The Zn-Co CMA coatings offers better corrosion resistance when the number of layers is increased and the top layer of the coating possess higher concentration of cobalt. Thangaraj *et al.*/35/ have demonstrated that the corrosion resistance of Zn-Co CMA coatings can be optimized by proper manipulation of the deposition conditions and the structure of the coating.

3.4 Electrodeposited graded coatings

3.4.1 Ni-B graded coatings

The possibility of preparing ED Ni-B graded coating having a gradation in the boron content throughout the thickness of the coating has been explored by Krishnaveni /22/. The two possible approaches to prepare ED Ni-B graded coatings are: (i) by varying the concentration of DMAB in

the Watt's bath; and (ii) by varying the current density. The first approach has a major limitation – use of higher concentration of DMAB could destabilize the plating bath. The second approach, which involves the formation of ED Ni-B graded coatings by continuously varying the current density is more viable. Based on the plating rate as a function of current density and time, the ED Ni-B graded coating (thickness: 60 μm) is prepared by continuously decreasing the current density from 4 to 0.4 A/dm^2. In order to understand the gradation in the ED Ni-B coating, the microhardness of the coated layer is evaluated at every 10 micron interval. The hardness profile as a function of coating thickness is shown in Fig. 7. It is evident that with increase in coating thickness (decrease in current density) the hardness of the coating is increased. The ED Ni-B graded coating with a relatively hard outer layer is expected to offer a better wear resistance. Much remains to be explored on ED Ni-B graded coatings.

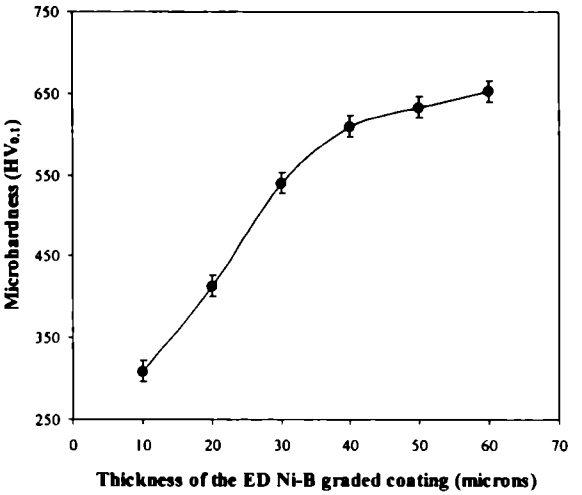

Fig. 7: Variation in microhardness of ED Ni-B graded coating as a function of its thickness (adapted from /22/)

3.5 Electrodeposited composite coatings

3.5.1 Ni-Si_3N_4, Ni-fly ash and Ni-calcium fluoride composite coatings

Ramesh *et al.* /36/ have studied the formation of nickel composite coatings on mild steel substrates by sediment electro-co-deposition

technique. Silicon nitride (α-type, 1 μm), fly ash (5 to 25 μm) and calcium fluoride powders (1 to 5 μm) are used as the reinforcements. During plating intermittent stirring of the plating bath with a quiescent period of 15 s and a stirring period of 10 s is used to disperse the particles. The sediment electro-co-deposition technique with intermittent stirring of the plating bath enables uniform distribution of the particles in the ED Ni matrix. The composite coatings exhibit low degree of porosity and also lesser tendency of agglomeration of the particles. Incorporation of silicon nitride and fly ash in the ED Ni matrix increases the hardness whereas a decrease in hardness is observed when calcium fluoride particles are incorporated (Table 3). All the composite coatings exhibit a lower coefficient of friction and better wear resistance when compared with nickel coatings at all loads and sliding velocities studied. ED Ni–calcium fluoride composite coatings possess the lowest coefficient of friction and wear rates. Ramesh *et al.* /36/ have also proposed a model for predicting the wear rate of ED Ni-composite coatings. The predicted wear rates based on the proposed model are found to be in reasonable agreement with the measured data.

Table 3
Comparison of the predicted and measured wear rate of composite coatings (adapted from /36/)

Coating composition	Sliding Velocity	Contact pressure	Wear rates (x 10^{-5}) $mm^3/(Nm)$	
			Predicted	Experimental
Nickel - 7.75 vol.% Si_3N_4	1.57	1.23	4.63	3.85
Nickel - 7.75 vol.% Si_3N_4	1.57	1.23	4.03	3.57
Nickel - 7.75 vol.% Si_3N_4	1.57	1.23	2.82	2.86
Nickel - 40.0 vol.% fly ash	1.57	1.23	1.55	1.52
Nickel - 40.0 vol.% fly ash	1.73	1.23	1.09	1.47
Nickel - 40.0 vol.% fly ash	1.26	1.23	1.57	1.51
Nickel – 6.0 vol.% CaF_2	1.57	1.23	1.83	1.45
Nickel – 6.0 vol.% CaF_2	1.57	1.23	0.53	0.70
Nickel – 6.0 vol.% CaF_2	1.26	1.10	0.43	0.39

3.5.2 Ni-B-Si_3N_4 composite coating

The formation of Ni-B-Si_3N_4 composite coating by electrodeposition technique and evaluation of its characteristic properties is studied by Krishnaveni *et al.* /37/. The Ni-B-Si_3N_4 composite coating is prepared by dispersing the Si_3N_4 particles in DMAB modified Watt's nickel plating bath. The maximum level of incorporation of Si_3N_4 particles in ED Ni-B matrix is obtained at a bath loading of 50 g/l and at a current density of 1 A/dm^2 and it contains 89.6 wt.% Ni; 2.4 wt.% B and 8 wt.% Si_3N_4. The incorporation of Si_3N_4 particles in the ED Ni-B matrix increases the surface roughness (R_a =1.17 μm) of the coatings (Fig. 8(a)). The surface morphology of the composite coating exhibits uniform distribution of the Si_3N_4 particles in the ED Ni-B matrix (Fig. 8(b)). Incorporation of Si_3N_4 particles in the ED Ni-B matrix causes a change in crystal orientation. The grain size of ED Ni-B-Si_3N_4 composite coating is 6 to 8 nm in as-plated condition and it increases to 12 to 14 nm after heat-treatment at 400 °C for 1 hour.

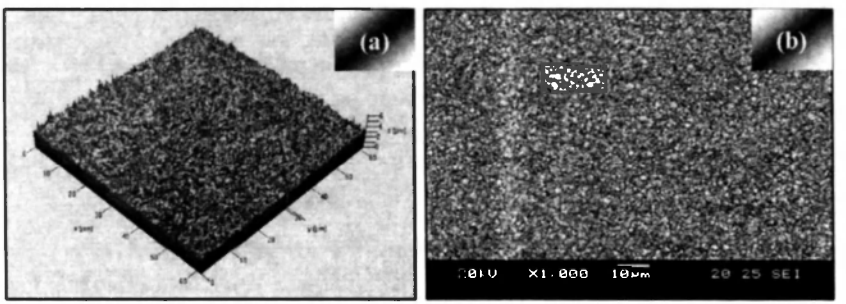

Fig. 8: 3-Dimensional view of the surface topography (a) and surface morphology (b) of Ni-B-Si_3N_4 composite coating electrodeposited at 1 A/dm^2 (adapted from /22/)

The microhardness of as-plated ED Ni-B-Si_3N_4 composite coating is 640 $HV_{0.1}$ and it increases to 955 $HV_{0.1}$ when the coating is heat-treated at 400 °C for 1 hour. The increase in microhardness is due to the combination of solid solution hardening of the ED Ni-B matrix and dispersion hardening induced by the incorporated Si_3N_4 particles in the matrix. The wear resistance of ED Ni-B-Si_3N_4 composite coating is evaluated by Krishnaveni *et al.* /38/ and compared with that of ED Ni-B coating. The wear resistance of ED Ni-B-Si_3N_4 composite coatings is relatively higher than that of ED Ni-B coatings, both in as-plated and heat-treated conditions due to the combination

of solid solution hardening of the matrix and dispersion hardening induced by particle incorporation. The wear resistance is higher for heat-treated ED Ni-B-Si_3N_4 composite coatings compared to those obtained in as-plated condition. The wear mechanism of ED Ni-B-Si_3N_4 composite coatings is also similar to that of ED Ni-B coatings - intensive plastic deformation of the coating due to the ploughing action of the hard counter disk. The nanocrystalline nature is primarily responsible for the corrosion behaviour of ED Ni-B-Si_3N_4 composite coatings in their as-plated condition. The corrosion resistance decreases further up on heat-treatment due to the crystallization of the coating, increase in the grain boundary region and formation of nickel boride phases. EIS studies indicate that the electrolyte has penetrated via the micropores in the ED Ni-B-Si_3N_4 composite coatings. The corrosion resistance of ED Ni-B-Si_3N_4 composite coating is relatively higher than ED Ni-B coatings, both in as-plated and heat-treated conditions, due to the decrease in the effective metallic area prone to corrosion.

3.5.3 Ni-CeO_2 composite coatings

Ni-CeO_2 nanocomposite coating is prepared by electrodeposition using a nickel sulphamate bath in the current density range of 0.23-5.4 A/dm^2 and its hardness wear resistance and corrosion resistance are evaluated by Aruna *et al.* /39/. The incorporation of CeO_2 particles in the ED Ni matrix increases the microhardness of the matrix. ED Ni-CeO_2 composite coatings prepared at 5.4 A/dm^2 exhibits the highest microhardness value of 508 $HK_{0.05}$. The ED Ni-CeO_2 composite coating exhibit a lower i_{corr} value (0.37 $\mu A/cm^2$) compared to ED pure Ni (0.68 $\mu A/cm^2$), indicating its better corrosion protective ability. The ED Ni-CeO_2 composite coating exhibits a low coefficient of friction compared to ED pure Ni initially. The wear coefficients calculated for ED Ni-CeO_2 and ED Ni coatings are 5.10×10^{-7} and 3.94×10^{-7}, respectively, which indicates that both ED Ni and Ni-CeO_2 coatings have undergone mild adhesive wear of burnishing type.

3.5.4 Ni-WC composite coatings

Surender *et al.* /40, 41/ have studied the formation of Ni–WC composite coating on mild steel by electrodeposition using Watt's bath. The electrochemical behaviour of ED Ni-WC composite coated mild steel is assessed using 0.1 M H_2SO_4 as the electrolyte solution /40/ and the tribological behaviour of the coating is evaluated using small amplitude

reciprocating friction wear tester /41/. The optimum conditions for the deposition of ED Ni-WC composite coating (i.e., uniform distribution of WC and uniform thickness) are as follows: current density: 0.2 A/cm^2; bath load: 2 g/l; and temperature: 50°C. The incorporation of WC in the ED Ni matrix did not exert any significant influence on the polarization behavior. The active-passive behavior is observed for ED pure Ni as well as ED Ni-WC composite coatings. However, the stability of the passive film formed by ED Ni-WC composite coating is significantly affected, which is manifested by a positive shift in the passivation potential, reduction in the passive range, and higher passive current densities compared to the pure Ni matrix. The electrochemical behaviour of ED Ni-WC composite coating suggests that the nature of passive film that from on it is defective compared to that form on ED pure Ni coating. The incorporation of WC in the ED Ni matrix increases the microhardness and the extent of increase is a function of the level of incorporation of the WC particles. The tribological behaviour of ED Ni–WC composite coating is also found to be a function of the level of incorporation of WC particles in the ED Ni matrix. The ED Ni-WC composite coating with an incorporation level of 37 wt% WC particles results in a much lower coefficient of friction (COF) of 0.34, when compared with pure Ni (COF 0.62) and mild steel (COF 0.54).

3.5.5 Ni-diamond and Ni-Co-diamond composite coatings

Malathy Pushpavanam *et al.* /42/ have studied the formation of Ni-diamond and Ni-Co-diamond composite coatings on mild steel by sediment electro-codeposition technique and evaluated their tribological properties. The Ni-diamond and Ni-co-diamond composite coatings are prepared using Watt's bath and cobalt modified Watt's bath in which natural diamond powders (size: 6 to 12 μm) are dispersed in them. Addition of cobalt to Watt's bath increases the level of incorporation of diamond powders, enables their uniform distribution, reduces their agglomeration in the metal matrix and decreases the surface roughness of the composite coating. Incorporation of diamond powder in both ED Ni and Ni-Co matrices increases the hardness. However, higher hardness is exhibited by ED Ni-Co-diamond composite coatings due to the higher level of incorporation of diamond particles. Both Ni- diamond and Ni-Co-diamond composite coatings exhibit lower wear rate compared to their pure metallic counterparts. Among the composite coatings, the wear rate of

Ni-Co-diamond composite coating is approximately three times lower than that of Ni-diamond composite coating. Besides the higher level of incorporation of diamond particles, the higher hardness of the Ni-Co matrix compared to pure nickel matrix could also be a contributing factor for the better anti-wear performance of the ED Ni-Co-diamond composite coating.

3.5.6 Ni-SiC and Ni-Co-SiC nanocomposite coatings

Meenu Srivastava *et al.* /43/ have studied the formation of Ni-SiC and Ni-Co-SiC nanocomposite coatings from an additive free sulphamate bath by electrodeposition and evaluated their microstructure, preferred orientation, surface morphology and wear behaviour. The matrix effect and the level of incorporation of the nano SiC particles on the hardness and wear resistance are studied in comparison with pure Ni coating. Incorporation of nano SiC particles in ED Ni matrix modifies the texture from the soft [100] mode to the mixed [211] mode. ED pure Ni deposit exhibits a crystallite size of 27 nm. Co-deposition of 1.4 wt.% nano SiC particles in the ED Ni matrix reduce the crystallite size to 11 nm. ED pure Ni deposit exhibits irregular polyhedral crystals whereas incorporation of nano SiC particles modifies it to spherical crystals. Two Ni–Co alloy matrices exhibiting different lattice structures, namely, Ni–28Co and Ni–70Co were used to study the formation of nanocomposite coating. The incorporation of nano-SiC particles in Ni-28Co and Ni-70Co alloy matrices alters the dense spherically smooth surface to a rough nodular morphology. However, the extent of agglomeration of SiC particles is less compared to Ni-SiC composite coatings. Incorporation of nano SiC particles in the Ni-28Co alloy matrix changed the preferred orientation from (200) to (100), similar to that observed in pure Ni matrix whereas the Ni-70Co alloy matrix exhibits a *hcp* lattice structure with a preferred (002) reflection. Incorporation of nano SiC particles in the Ni-28Co alloy matrix decreases the crystallite size from 27 nm to 7 nm (reference to (200) reflection) whereas in Ni–70Co alloy matrix the crystallite size is decreased from 20 to 10 nm (reference to (110) reflection).

Co-deposition of nano-SiC particles increases the microhardness of the Ni–28Co alloy matrix, similar to that observed in pure Ni matrix whereas the hardness of Ni-70Co alloy matrix remains unaltered, suggesting that the nano SiC particles do not contribute to the hardening mechanism of Ni-70Co alloy matrix unlike, pure Ni and Ni–28Co matrices. The Ni-70Co alloy matrix exhibits lower coefficient of friction due to the hcp lattice structure. The

coefficient of friction of Ni-SiC and Ni–28Co-SiC nano-composite coatings is almost similar. The volumetric wear loss of Ni–SiC and Ni–28Co–SiC composite coatings is in accordance with the Archard's law. The Ni–70Co-SiC composite coating exhibit the least wear loss which indicates its superior tribological properties compared to Ni-SiC and Ni-28Co-SiC composite coatings. The Ni–70Co-SiC composite coating follows the reverse Archard's law. The nature of wear is identified as adhesive wear.

3.5.7 Zn-CNT composite coating

In recent years, the carbon nanotubes (CNTs) have attracted tremendous interest from fundamental and applied perspectives. Praveen *et al.* /44/ have studied electrodeposition of Zn-CNT composite coating and its corrosion behavior. The Zn-CNT composite coating is prepared by electrodeposition using a sulphate based bath in which the multiwalled CNTs (diameter: 10-20 nm; length: 10-50 μm) are dispersed with the help of cetyl trimethyl ammonium bromide. The thickness of Zn-CNT composite coatings is in the range 15–20 μm. The corrosion behaviour of Zn-CNT composite coatings are evaluated using immersion, salt spray and electrochemical tests and their performance is compared with that of pure Zn coatings. The study reveals that the Zn-CNT composite coatings offer better corrosion resistance compared to pure zinc coating. The inclusion of CNTs in the electrodeposited zinc matrix significantly reduces the porous nature of the pure zinc coating. The CNTs incorporated in the zinc matrix fills the crevices, gaps, and micro holes on the surface of the deposit and acts as a physical barrier to corrosion.

3.5.8 Ni-SiC, Ni-Al_2O_3 and Ni-SiO_2 composite coatings using aqueous-organic bath

Electrodeposition of composite coatings is usually carried out by dispersing the second phase particles in aqueous plating bath. Singh and Pinky Pandey /45/ have explored the formation of Ni-SiC, Ni-Al_2O_3 and Ni-SiO_2 composite coatings by electrodeposition using a bath containing nickel sulphamate and boric acid in a 50:50 mixture of diethanolamine and water. The co-deposition of SiC, Al_2O_3 and SiO_2 particles is found to be a function of the flux of the particles to the cathode surface which in turn depends on the particle size, particle concentration in the solution, the rotation rate, particle diffusion coefficient and electrode geometry, which is quite similar to that of the aqueous bath. However, the level of incorporation

of these ceramic particles in the ED Ni matrix increases with an increase in current density, which is different from that of the aqueous bath. Among the three types of particles, codeposition of SiC seemed to be favourable in comparison with Al_2O_3 or SiO_2 under similar experimental conditions. The aqueous-organic bath is considered to have some advantages over the aqueous bath:

(i) The aqueous-organic bath has high viscosity and high tendency of metal complexation
(ii) The suspension of the ceramic particles in the aqueous-organic bath is stable for a longer period of time
(iii) The physical properties of the aqueous-organic bath could influence the gravitational force, particle diffusion coefficient, etc., i.e. flux of the particles to the electrode surface
(iv) The aqueous-organic bath enables the formation of composite coatings under high current densities and turbulent flow conditions.

The incorporation of SiC, Al_2O_3 and SiO_2 in the ED Ni matrix exhibit a dependence of texture depending on the type of particles incorporated. ED Ni-SiC composite coating exhibits a preferred orientation along Ni (200), ED Ni-Al_2O_3 composite coating exhibits a preferred orientation along Ni (111), whereas no preferred orientation is observed for ED Ni–SiO_2 composite coating.

3.5.9 Ni-nano NiO composite coatings

Electro- and electroless plated nickel electrodes have been used as sensors for the determination of alcohols, acetylcholine, etc. The sensing performance of these electrodes can be considerably improved by increasing their surface area. Shibli *et al.* /46/ have explored the possibility of preparing Ni-nano NiO composite coatings by electrodeposition and evaluated their suitability as a biosensor for estimating acetylcholine (ACh), an important neurotransmitter. The ED Ni-Nano NiO composite coating is deposited on graphite electrodes using Watt's bath in which the nano NiO particles (0-1 g/l) are dispersed in it. The ED Ni-nano NiO composite coating prepared using 0.1 g/l of nano NiO powders exhibit a response time of 8 seconds for the estimation of ACh, which is much lesser than the response time of 23 seconds observed for ED pure Ni coating and other type of sensors. The sensitivity of the ED Ni-nano NiO composite coated electrodes is found to be

34.88 $\mu A/(\mu Mcm^2)$. The adhesion of ED Ni-nano NiO composite coating is found to be good even after repeated usage for sensing measurements. The low response time and high sensitivity exhibited by ED Ni-nano NiO composite coating prepared using 0.1 g/l of nano NiO powders is due to the increase in surface area and surface activity. However, the response time is found to be higher for ED Ni-nano NiO composite coatings prepared using nano NiO powders at > 0.1 g/l.

4. ELECTROLESS PLATING

The recent developments in electroless (EL) plating include the choice of the right stabilizer for EL plating bath, the possibility of utilizing EL Ni-P coatings for corrosion protection of reinforcement steel and as an interlayer for PVD hard coatings, blackened EL Ni-P coating as high absorptance coating for space applications, development of EL Ni-B coatings using alkaline-borohydride reduced EL plating bath at high and low temperatures, EL Ni-P and Ni-B coatings for corrosion protection of Nd-Fe-B magnet, EL Ni-P/Ni-B duplex coatings, EL Ni-P graded coatings, EL Ni-P and Ni-B polyalloy coatings, EL Ni-P and Ni-B based composite coatings and EL nickel plating of ceramic powders for many functional applications.

4.1 EL Ni-P coatings

4.1.1 Choice of stabilizer – lead acetate vs. thiourea

In general, EL Ni–high P deposits are amorphous in nature, exhibit good corrosion resistance and solderability. They are usually prepared from acidic baths at high temperatures of the order of 90 °C. At such high temperatures, nickel phosphite, formed due to the oxidation of hypophosphite is likely to precipitate in the bath. Since EL nickel baths are highly sensitive to impurities, maintaining the bath stability is very critical and warrants the addition of stabilizers to avoid decomposition of the plating bath. Thiourea and lead acetate are the most commonly used stabilizers in EL plating baths. Since the toxicity of lead is not desirable, thiourea is often used as a substitute for lead acetate. However, lead acetate and thiourea would behave distinctly in terms of the rate of deposition, crystallinity of the coating,

morphological feature and corrosion resistance. Hence, the use of thiourea in place of lead acetate requires careful study. Baskaran *et al.* /47/ have studied the effect of thiourea and lead acetate on the formation and characteristics of EL Ni–P coatings from an acidic hypophosphite-reduced EL plating bath.

Addition of thiourea accelerates the rate of deposition of EL Ni-P coating up to 0.8 ppm and started to inhibit when the concentration of thiourea is $\geq$ 1 ppm. Addition of lead acetate inhibits the rate of deposition of EL Ni-P deposits even at 0.5 ppm and the extent of inhibition is increased when the concentration of lead acetate is > 1 ppm. Addition of lead acetate (1 ppm) due to its inhibiting effect on the cathodic reduction of nickel ions causes a slight increase in the phosphorus content (from 11.23 to 11.96 wt.%) of the coating compared to the coating obtained from the bath without any additive. However, addition of thiourea (0.8 ppm) due to their ability to increase the rate of deposition causes a slight decrease in the phosphorus content (from 11.23 to 10.47 wt.%), compared to the coating obtained from the bath without any additive. There is a greater tendency for the deposit to form amorphous structure when lead acetate is used as the stabilizer. In contrast, EL Ni–P coatings obtained in presence of thiourea are relatively less amorphous. EL Ni–P coatings obtained in presence of thiourea exhibit a nodular feature with a typical cauliflower like structure due to the rapid formation of nuclei and subsequent growth of the Ni–P deposit. In contrast, EL Ni–P coating obtained in presence of lead acetate is relatively smooth (Fig. 9). The EL Ni-P deposits obtained in presence of thiourea and lead acetate offers less corrosion protection compared to the coating obtained from additive free bath. The decrease in corrosion resistance of EL Ni-P coatings obtained in presence of thiourea and lead acetate could possibly be due to the codeposition of sulphur and lead in the respective coatings and due to the increase in surface roughness. Since the addition of lead acetate and thiourea could influence the plating rate, crystallinity, surface morphology, structural, thermal and magnetic properties and, corrosion resistance, the choice of thiourea as a substitute for lead acetate should be made only after a careful study.

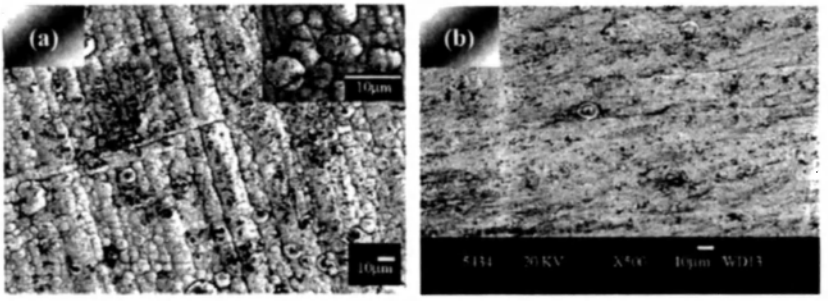

Fig. 9: Surface morphology of EL Ni–P coatings obtained from acidic hypophosphite-reduced EL plating bath in presence of (a) 0.8 ppm of thiourea and (b) 1 ppm of lead acetate (Reprinted from *Materials Chemistry and Physics*, Vol. 99(1), I. Baskaran, T.S.N. Sankara Narayanan and A. Stephen, Effect of accelerators and stabilizers on the formation and characteristics of EL Ni–P deposits, pp. 117-126 (2006) with permission from Elsevier Science)

4.1.2 EL Ni-P coating for corrosion protection of reinforcement steel

The use of EL Ni-P coatings for protecting the corrosion of reinforcement steel bars in simulated chloride-contaminated concrete environment is studied by Singh and Rita Ghosh /48/. Sanchez *et al.* /49/ have also studied the performance of EL nickel coatings for reinforcing steel in chloride contaminated concrete. Singh and Rita Ghosh /48/ have evaluated the performance of both high phosphorus (HIPEN) (P: 16.10 %) and medium phosphorus (MEPEN) (P: 8 %) EL nickel coatings in simulate pore solution (SPS) having 1 M chloride ions with OH^-/Cl^- ratio of 0.13, which is an extremely aggressive condition for corrosion of reinforcement bars embedded in concrete. MEPEN coating imparts a very high degree of corrosion protection compared to HIPEN coating in SPS + 1 M Cl^- solution. The high corrosion resistance offered by MEPEN is attributed to the development of a pore-free passive film consists of Ni_2O_3 and Ni_5P_2. Heat treatment of MEPEN at 600 °C in air has a deleterious effect on the corrosion resistance. The decrease in corrosion resistance following heat-treatment is attributed due to the contamination of the Ni-P coating by iron and silicon, which are diffused from the steel substrate.

4.1.3 EL Ni-P coating as an interlayer for PVD hard coatings

Hard coatings deposited by physical vapor deposition (PVD) technique exhibit good wear resistance, chemical inertness and high thermal stability. However, the corrosion resistance offered by thin PVD coatings is low due to the defects in the coating such as pores, pinholes and cracks, which might be formed during the deposition. The columnar microstructure of these coatings also weakens their corrosion protective ability. The deposition of an interlayer would improve the corrosion resistance. The interlayer can be produced by electro/electroless deposition (e.g., Ni) or by physical vapor deposition (e.g., Ti, Cr). The metallic interlayer deposited by PVD improves the adhesion and the corrosion properties. But it is not completely free from defects. EL nickel, however, offers better resistance to corrosion, wear and abrasion and provides uniformity in thickness of the deposits. Hence, a combination of EL nickel interlayer and the PVD hard coating is expected to improve both the mechanical and corrosion properties of the duplex coating. The influence of EL nickel as an additional interlayer on the corrosion resistance of single layer TiN, CrN, TiAlN and multilayer TiAlN/CrN coatings, deposited on steel substrates using a multi target reactive direct current (dc) magnetron sputtering process, in 3.5% NaCl solution is evaluated by William Grips *et al.* /50/. The thickness of single and multilayer hard coatings is about 1.5 μm. About 0.5 μm thick Cr interlayer is incorporated between the substrate and the film for improved adhesion. EL Ni-P coating, about 5 μm thick, is deposited as an additional interlayer. The EL Ni-P interlayer on the sample surface has provided more homogeneous, uniform and denser structure, resulting in the improved corrosion resistance. The hard coatings deposited with EL Ni-P interlayer reduce the porosity value by three to four orders of magnitude lower than the coatings without EL Ni-P interlayer. The deposition of a 5 μm thick EL Ni-P coating as interlayer increases the corrosion resistance of both single layer TiN, CrN and TiAlN coatings as well as TiAlN/CrN multilayer coatings. The improvement in corrosion resistance is due to the decrease in defect density of the coating by the introduction of EL Ni-P coating as interlayer.

4.1.4 Blackened EL Ni-P coatings as high absorptance coating for space applications

Ultra high absorptance black coatings are of paramount importance in the design of terrestrial and space-borne optical instruments and sensors used for

measurements in ultra-violet, visible and infrared spectral regions. These coatings are extremely useful to improve the absorptance of thermal detectors and to suppress the unwanted reflections or scattered light in optical systems, like telescope housing and baffles where stray light reduction is vital. Saxena *et al.* /51/ have developed a simple chemical immersion process of blackening of EL Ni-P coating to provide ultra high absorptance coating on aluminium substrate. Blackening of the EL Ni-P coating is performed by immersion treatment in three different acid formulations, namely, (i) nitric acid (9 M); (ii) a mixture of sulphuric (6 M) and nitric acid (4 M); and (iii) a mixture of nitric acid (1.1 M), sulphuric acid (0.3 M) and potassium permanganate (0.1 M). The morphology of the black nickel deposits is found to be a function of the phosphorous content. EL Ni-low P coating yields a well pronounced 'crater' morphology whereas a 'stalagmite-like' morphology is obtained for EL Ni-high P coating. EL Ni–low P coating is etched more completely with large crater formation as major portions of the coating is dissolved during etching. In contrast, it is more difficult to etch the large swaths of EL Ni–high P coating. The high absorptance of the black nickel deposits is associated with its unique surface morphology consisting of a dense array of microscopic, conical pores perpendicular to the surface. This structure produced by the selective etching of the EL Ni–P coating, which acts as light traps and capable of absorbing 99.5% light in the solar region (300 to 2300 nm). The pore diameter, pore depth and pore spacing range from a fraction of micrometer to a few micrometers or about a fraction to several wavelengths of light. Consequently, the pores trap any incident light in wide spectral range. The black color of Ni–P coating is due to this unique surface morphology as well to the formation of nickel oxides (NiO, Ni_2O_3) and some nickel phosphate.

The phosphorus content of the EL Ni deposit, thickness of the deposit, type of oxidizing acids used for etching, temperature of the etching solution and etching time play a significant role in achieving higher absorptance of the coating after blackening. EL Ni-high P coatings are more resistant to acid etching, requires higher concentration of oxidizing acids and they are not suitable for blackening to achieve a high solar absorptance. Lower the initial phosphorous content in the EL nickel, the greater the extent of the etching and lower the reflectance of the resulting surface. The optimum results are obtained when the EL Ni-P coatings are prepared using a bath pH of 4.7. Since strong oxidizing acids are used for etching, the thickness of EL nickel

could decrease by about 5 μm during the blackening process. Hence, the optimum thickness of EL Ni-P coating to achieve the high solar absorptance after etching is 30 ± 2 μm. At low temperatures, the etching rate is slow and the solar absorptance of resultant coatings is lower. Increase in temperature though enables a decrease in processing time might result in powdery deposit due to the heavy dissolution. The optimum temperatures recommended for the etching solutions (i), (ii) and (iii) are 40, 60 and 40 °C, respectively. Lower etching time yields non-uniform black coating with low solar absorptance whereas increase in etching time beyond a certain range results in powdery coating or peeling from the edges due to excessive dissolution of coating. The blackened EL Ni-P coatings possess excellent adhesion, exhibit good stability in corrosive environment, better thermal stability, good stability in adverse space conditions and provides high solar absorber in the order of 0.995. These surfaces are extremely suitable to improve the absorptance of thermal detectors and to minimize the effect of stray and scattered light in optical instruments and sensors. The blackened EL nickel coating is extremely suitable as a solar absorber coating for space and allied application.

4.2 Electroless Ni-B coatings

4.2.1 EL Ni-B coatings using a high temperature bath

The formation of EL Ni-B coating and evaluation of its characteristic properties has been reported by Sankara Narayanan and Seshadri /52/, Krishnaveni /22/ and Krishnaveni *et al.* /53/. The EL Ni-B coating is prepared using an alkaline borohydride-reduced EL plating bath. The instability of borohydride at pH <12 allows only a narrow window of operation. To achieve better bath stability and higher deposition rate, addition of thallium compounds as stabilizers is essential. The rate of deposition of EL Ni-B coatings is found to be a function of bath temperature and molar ratio of ethylenediamine to nickel. The rate of deposition of EL Ni-B coating decreases with increase in plating time. The EL Ni-B coatings are matte in appearance, dark gray in colour and it contains 93.2 wt.% nickel, 6.5 wt.% boron and 0.3 wt.% thallium. The morphology of EL Ni-B coatings resembles a typical cauliflower type feature (Fig. 10).

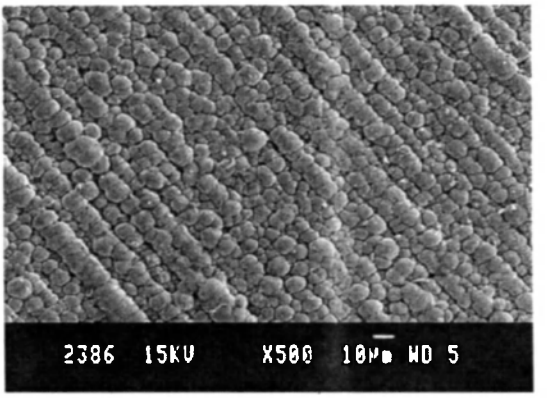

Fig. 10: Surface morphology of EL Ni-B coating (Reprinted from *Surface and Coatings Technology*, Vol. 190, K. Krishnaveni, T.S.N. Sankara Narayanan and S.K. Seshadri, Electroless Ni–B coatings: preparation and evaluation of hardness and wear resistance, pp. 115-121 (2005) with permission from Elsevier Science)

The EL Ni-B coating is amorphous in as-plated condition whereas it becomes crystalline upon heat-treatment, with the formation of Ni, Ni_3B phases at 350 °C and Ni, Ni_3B and Ni_2B phases at 450 °C. Heat-treatment at 600°C for 1 hour causes conversion of the Ni_2B phase into the more stable Ni_3B phase. The grain size of EL Ni-B coatings is 2 to 3 nm in as-plated condition and it increases to 8 to 10 nm after heat-treatment at 450 °C for 1 hour. The microhardness of EL Ni-B coating is 570 $HV_{0.1}$ for as-plated coatings and 908 $HV_{0.1}$ for coatings heat-treated at 450 °C for 1 hour. The hardness vs. heat treatment temperature curve exhibits two maxima, the first maximum occurs at 350 °C whereas the second maximum occurs at 450 °C. Beyond 450 °C, the hardness decreases. The increase in hardness is due to the precipitation of nickel borides, Ni_3B and Ni_2B. The formation of these phases is confirmed by XRD measurement. At temperatures above 450 °C, the coating begins to soften as a result of coarsening of the Ni_3B particles, which thereby reduces the number of hardening sites.

The wear resistance of heat-treated EL Ni-B coating is relatively higher than that of the as-plated coatings. Adhesive wear appears to be the most likely mechanism during the wear process of EL Ni-B coatings. EL Ni-B coatings demonstrate a moderate corrosion resistance in 3.5% sodium

chloride solution. The extent of corrosion resistance offered by EL Ni-B coatings is relatively less compared to EL Ni-9 wt.% P coating. Surface heterogeneity and columnar structure are primarily responsible for the lower corrosion resistance of EL Ni-B coatings in their as-plated condition. The corrosion resistance decreases further up on heat-treatment due to the crystallization of the coating, increase in the grain boundary region and formation of nickel boride phases. EIS studies indicate that the electrolyte has penetrated through the pores in the EL Ni-B coating. VSM studies performed on EL Ni-B films reveal that they are non-magnetic in as-plated condition and started to exhibit magnetic activity consequent to the formation of crystalline nickel phase.

4.2.2 EL Ni-B coatings using a low temperature bath

Electroless plating of components used in electronic applications require a plating bath that operates at a relatively lower temperature. Hence, DMAB-reduced EL plating baths are commonly used for these applications. To achieve better reduction efficiency and cost-effectiveness, borohydride-reduced baths could also be explored for components used in electronic applications. As most of the borohydride- reduced EL plating baths reported in literature operate at very high temperature of the order of 90- 95°C, the development of plating baths that operate at relatively lower temperatures is warranted for processing components used in electronic applications. In this perspective, Baskaran *et al.* /54/ have developed a borohydride-reduced EL nickel plating bath using ethylenediamine and disodium tartarate as complexing agents, sodium borohydride as the reducing agent and thallium acetate as the stabilizer in the EL plating bath that operate at 45 °C.

The plating rate of EL Ni-B coatings obtained using 1 g/l of $NaBH_4$ is 10 μm/hour. The rate of deposition of EL Ni-B coating at 95 °C is about 18 to 20 μm/hour at 0.8 g/l of $NaBH_4$ and 25 to 30 μm/hour at 1.05 g/l of $NaBH_4$. Though the rate of deposition of EL Ni-B coatings obtained using the low temperature bath is low compared to that obtained from high temperature bath, there is further room to improve the rate of deposition with the addition of suitable accelerators in the bath. The EL Ni–B coatings are matte in appearance and dark gray in colour. The coatings are uniform and they consist of agglomerates of nickel that are randomly distributed. The morphology resembles a typical cauliflower type feature (Fig. 11).

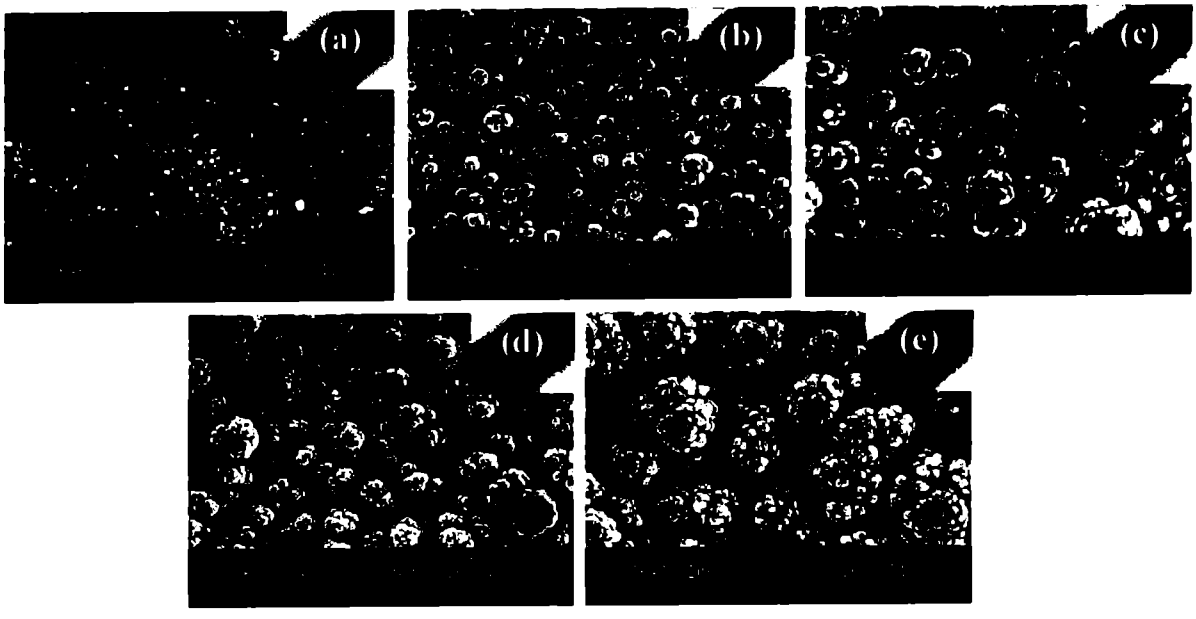

Fig. 11: Scanning electron micrograph of EL Ni–B coatings obtained from the low temperature bath using different concentrations of $NaBH_4$ (a) 0.2 g/l $NaBH_4$ (b) 0.4 g/l $NaBH_4$ (c) 0.6 g/l $NaBH_4$ (d) 0.8 g/l $NaBH_4$ and (e) 1.0 g/l $NaBH_4$ (Reprinted from *Surface and Coatings Technology*, Vol. 200(24), I. Baskaran, R. Sakthikumar, T.S.N. Sankara Narayanan and A. Stephen, Formation of electroless Ni–B coatings using low temperature bath and evaluation of their characteristic properties, pp. 6888-6894 (2006) with permission from Elsevier Science)

The size of the nodules increases with increase in concentration of $NaBH_4$ in the plating bath. These nodules combined to form a granular type structure, which makes the EL Ni–B coatings naturally lubricious and enables them to achieve higher wear resistance by reducing the surface contact. The structure, phase transformation behaviour and magnetic properties are found to be a function of the boron content of the coating. Coatings obtained using low concentration of $NaBH_4$ (0.4 g/l) are crystalline whereas those obtained using a higher concentration of $NaBH_4$ (1.0 g/l) possess a mixture of amorphous and crystalline phases, suggesting a decrease in crystallinity with increase in boron content of the coating. DSC traces exhibit a single exothermic peak around 300 °C for coatings prepared using 0.4 g/l of $NaBH_4$ and two distinct exothermic peaks around 300 and 420 °C for coatings prepared using 0.6 to 1 g/l of $NaBH_4$ corresponding to the phase transformation of crystalline nickel and Ni_3B phases at 300 °C and transformation of a higher phase compound to Ni_3B at 420 °C. EL Ni–B coating with higher boron content exhibits a lower saturation magnetization and vice-versa. Heat-treatment (400 °C/1 hour) increases the saturation magnetization values due to the crystallization of coatings.

4.2.3 EL Ni-P and Ni-B coatings for corrosion protection of Nd-Fe-B magnet

Permanent magnets are essential components in many of the electric, electronic and electromechanical devices to provide large magnetic fields without the expenditure of electrical power or the generation of heat. Among the four major families of permanent magnets, Nd-Fe-B magnets have received widespread acceptance due to their outstanding magnetic properties, namely, high remenance (11 kG), high coercivity (13 kOe) and high energy product (40 M GOe). The factors that determine the use of Nd-Fe-B magnets in a variety of applications are magnetization, irreversible losses due to high temperature use, corrosion resistance, shaping, structural integrity and mechanical properties. Nd-Fe-B magnet has two major limitations; its Curie temperature (312 °C) and operation temperature (80 °C) are relatively low; and its corrosion resistance in humid and/or chloride-containing environments is extremely low. These inherent limitations, especially the corrosion resistance, seriously impede and limit its applications. Attempts to improve the corrosion resistance of Nd-Fe-B magnets have been approached in two different routes: (i) addition of various alloying elements to the

magnet to modify its intrinsic corrosion properties; and (ii) application of metallic or non-metallic coatings to isolate the substrate from the environment. The right choice of coatings, which could improve the corrosion resistance without much deterioration in the magnetic properties, is the key in this area of research.

The deposition of EL Ni-P and Ni-B coatings using an acidic hypophosphite and alkaline borohydride-reduced EL plating baths on Nd-Fe-B magnet and evaluation of their corrosion protective ability is studied by Baskaran *et al.* /55/. The polarization curves of uncoated, EL Ni-P and Ni-B coated Nd-Fe-B magnet in 3.5% NaCl solution is shown in Fig. 12.

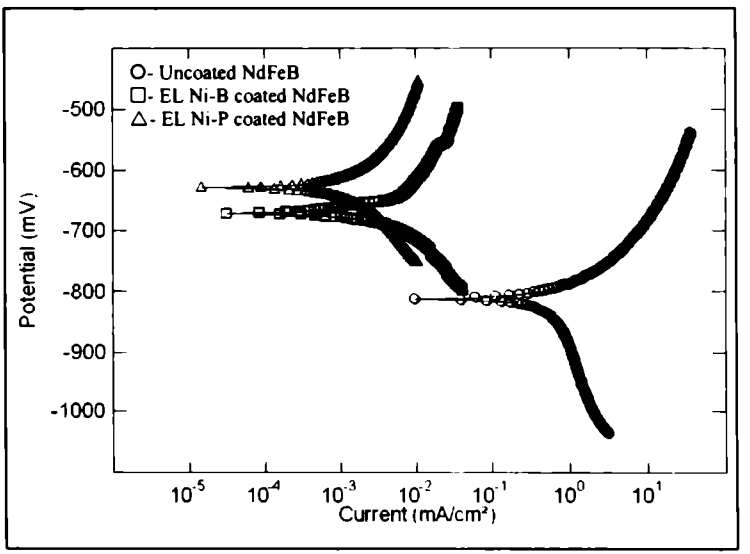

Fig. 12: Potentiodynamic polarization curves of uncoated and EL Ni-P and Ni-B coated Nd-Fe-B magnets (Potential in mV vs. SCE) (adapted from /55/).

The EL Ni-P and Ni-B coatings act as a barrier layer and improve the corrosion resistance of Nd-Fe-B magnet. The corrosion resistance of Nd-Fe-B magnet coated with EL Ni-B coating is relatively inferior compared to those coated with EL Ni-high P coating. The difference in corrosion resistance between the EL Ni-high P and EL Ni-B coated Nd-Fe-B magnets is mainly due to the difference in their structure. The passivation films that form on EL Ni-B coated surfaces are not as glassy or protective enough as

those that form on EL Ni-high P coatings. The phase boundaries, present in EL Ni-B coatings might also be responsible for causing discontinuity of the passivation film, which are the preferred sites for the initiation of corrosion process. Besides, the inhomogeneous distribution of boron and thallium throughout the EL Ni-B coating provides areas of different corrosion potential on the surface, which would lead to the formation of minute active/passive corrosion cells and accelerated the corrosion attack.

4.3 Electroless Ni-P/Ni-B duplex coatings

Sankara Narayanan *et al.* /56/ have explored the possibility of preparing EL Ni-P/Ni-B duplex coatings using dual baths (acidic hypophosphite- and alkaline borohydride-reduced EL nickel baths) with both Ni-P and Ni-B as inner layers and with varying single layer thickness. The duplex coatings are uniform and the compatibility between the layers is good. Scanning electron micrographs of the cross-section of EL Ni–B/Ni–P duplex coatings in as-plated and heat-treated (450 °C for 1 hour) conditions are shown in Fig. 13.

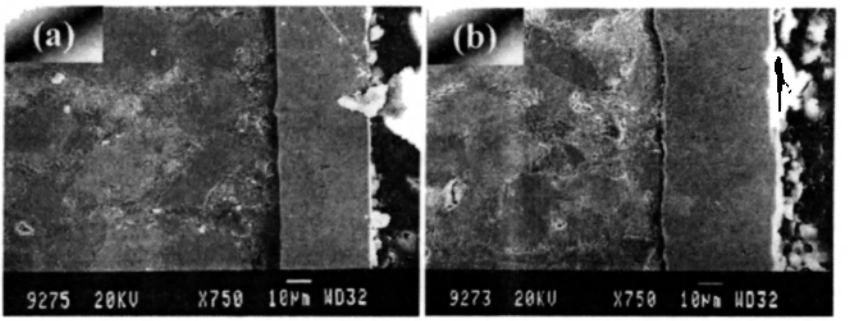

Fig. 13: Scanning electron micrographs of the cross-section of EL Ni–B/Ni–P duplex coatings (a) as-plated and (b) heat-treated at 450 °C for 1 hour (Reprinted from *Materials Chemistry and Physics*, Vol. 82, T.S.N. Sankara Narayanan, K. Krishnaveni and S.K. Seshadri, Electroless Ni-P/Ni-B duplex coatings: Preparation and evaluation of microhardness, wear and corrosion resistance, pp. 771-779 (2003) with permission from Elsevier Science).

The corrosion and wear resistance of EL Ni-P/Ni-B duplex coatings are better than EL Ni-P and Ni-B coatings of similar thickness (Table 4). EL Ni-P/Ni-B duplex coatings will be a useful replacement for EL Ni–B and

EL Ni–P coating, as they possess the desirable qualities of both types of coatings. If higher hardness and wear resistance are desired, then the duplex coating having EL Ni–B as the outer layer will be the ideal choice whereas the duplex coating having EL Ni–P as the outer layer is the preferred option where higher corrosion resistance is sought.

Table 4

Corrosion resistance of EL Ni-P, Ni-B, Ni-P/Ni-B and Ni-B/Ni-P duplex coatings in as-plated and heat-treated conditions in 3.5% NaCl (adapted from /56/)

System studied	Thickness (μm)	E_{corr} (mV vs. SCE)	i_{corr} (μA/cm^2)	R_{ct} (Ohms.cm^2)	C_{dl} (F) x 10^{-4}
EL Ni-P as-plated	20	-354	3.62	7960	1.85
EL Ni-P heat-treated	20	-492	6.89	6498	2.36
EL Ni-B as-plated	20	-508	9.15	3844	3.53
EL Ni-B heat treated	20	-519	14.60	1232	4.22
EL Ni-P/Ni-B duplex as-plated	10 + 10	-386	3.86	7638	1.89
EL Ni-P/Ni-B duplex heat-treated	10 + 10	-432	4.93	5339	2.44
EL Ni-B/Ni-P duplex as-plated	10 + 10	-311	2.46	10130	1.61
EL Ni-B/Ni-P duplex heat-treated	10 + 10	-356	3.24	7024	1.96

4.4 Electroless Ni-P graded coatings

Sankara Narayanan *et al.* /57/ have explored the possibility of preparing EL Ni-P graded coatings by sequential immersion in three different hypophosphite-reduced EL plating baths. One important aspect of depositing EL Ni-P graded coatings is the application of a nickel strike between each layer, so that the deposition proceeds without any hindrance when the substrate is sequentially immersed in EL plating baths. The graded EL Ni-P coatings are uniform and the compatibility between the three layers is good. The scanning micrograph of the cross-section of graded EL Ni–P (LMH)

coating is shown in Fig. 14. The EL Ni-P graded coatings offer a better corrosion resistance compared to EL Ni-P non-graded coatings. Among the two types of EL Ni-P graded coatings, the coating system with EL Ni-high P coating as the outer layer offers better corrosion resistance than its counterpart. However, the corrosion resistance of EL Ni-P graded coating with EL Ni-low P as the outer layer is better than that of EL Ni-low P coating, due to the barrier properties of the underlying Ni-medium P and Ni-high P layers (Table 5). Based on their ability to offer corrosion resistance the coatings can be ranked in the following order:

EL graded Ni-P(LMH) > EL Ni-high P > EL Ni-medium P > EL graded Ni-P(HML) > EL Ni-low P

Heat-treatment of EL Ni-P graded coatings is likely to modify the graded layers so that the gradation is lost. Hence the concept of graded EL Ni-P coatings is valid only in as-plated condition. Besides, heat-treatment (400 °C for 1 hour) drastically reduced the corrosion resistance of these coatings.

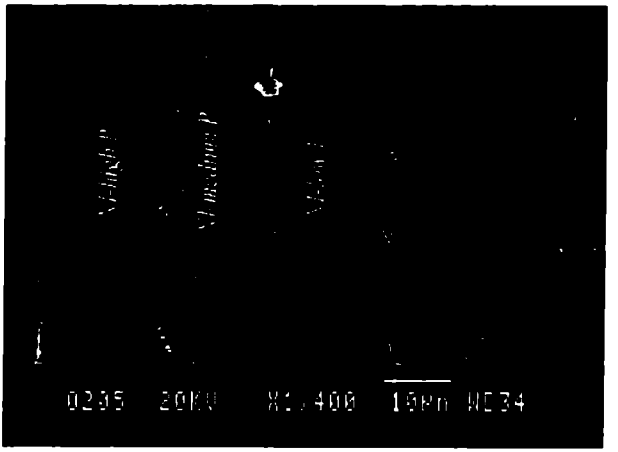

Fig. 14: Scanning electron micrograph of the cross-section of the graded EL Ni–P (LMH) coating (Reprinted from *Surface and Coatings Technology*, Vol. 200(11), T.S.N. Sankara Narayanan, I. Baskaran, K. Krishanaveni and S. Parthiban, Deposition of electroless Ni–P graded coatings and evaluation of their corrosion resistance, pp. 3438-3445 (2006) with permission from Elsevier Science)

Table 5

Corrosion resistance of non-graded and graded EL Ni-P coatings in 3.5% sodium chloride solution (adapted from /57/)

System studied	E_{corr} (mV vs. SCE)	i_{corr} ($\mu A/cm^2$)	R_{ct} ($K\Omega.cm^2$)	C_{dl} (μF)
EL Ni-Low P coating (L)	-536	4.22	6.90	289
EL Ni-Medium P coating (M)	-434	1.17	24.86	56
EL Ni-High P coating (H)	-411	0.60	37.45	49
EL Ni-P graded coating (LMH)*	-403	0.41	38.22	37
EL Ni-P graded coating (HML)*	-481	1.70	14.77	103

* LMH - Low-Medium-High P; HML – High-Medium-Low P.

4.5 Electroless Ni-P and Ni-B polyalloy coatings

4.5.1 Electroless Ni-Co-P and Ni-Co-B ternary alloy coatings

Sankara Narayanan *et al.* /58, 59/ have studied the formation of EL Ni-Co-P and Ni-Co-B ternary alloy coatings from alkaline citrate based plating baths using sodium hypophosphite and DMAB as the respective reducing agents with nickel to cobalt metallic ratios of 0.3, 0.5 and 0.7. The plating rate of EL Ni–Co–P and Ni-Co-B alloy coatings decreases with increase in metallic ratio ($CoSO_4/CoSO_4 + NiSO_4$) due to the higher catalytic activity of nickel compared to that of cobalt. With increase in metallic ratio, the cobalt content of both EL Ni-Co-P and Ni-Co-B alloy coatings increases with a simultaneous decrease in nickel content, while the phosphorus and boron content of the respective deposits decreases slightly (Fig. 15). The phosphorus and boron content of EL Co–Ni–P and Ni-Co-B alloy coatings increases with increase in concentration of nickel sulphate in the plating bath, with a corresponding increase in nickel content of these deposits, suggesting a higher level of codeposition of phosphorus and boron with nickel than cobalt. The study reveals that variation in metallic ratio provides a means of preparing Ni-Co-P/Ni-Co-B alloy coatings with varying contents of nickel, cobalt and phosphorus/boron.

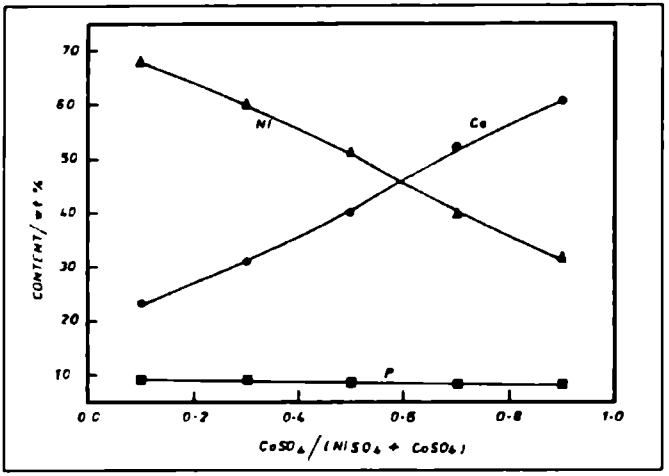

Fig. 15: Effect of metallic ratio ($CoSO_4/CoSO_4 + NiSO_4$) on the chemical composition of the EL Ni–Co–P ternary alloy deposit (Reprinted from *Surface and Coatings Technology*, Vol. 172, T.S.N. Sankara Narayanan, S. Selvakumar and A. Stephen, Electroless Ni–Co–P ternary alloy deposits: preparation and characteristics, pp. 298-307 (2003) with permission from Elsevier Science)

The EL Ni-Co-P and Ni–Co–B alloy coatings are amorphous in as-deposited condition. The DSC trace of EL Ni-Co-P alloy coating exhibits three distinct exothermic peaks, corresponding to the relaxation of lattice strain during the phase separation, the phase transformation of amorphous phase to nickel and nickel phosphide phases and the transformation of metastable phases to stable nickel phosphide phase. The DSC trace of EL Ni-Co-B alloy coating exhibits two exothermic peaks, corresponding to the separation of nickel phase from the amorphous matrix and formation of Co_3B phase. Annealing of EL Ni–Co–P alloy coating at different temperatures causes transformation of the amorphous to metastable and stable phases; annealing at 300 °C for 1 hour leads to the formation, Ni, Ni_3P and Ni_5P_2 phases; annealing at 400 °C for 1 hour leads to the formation of Ni, Ni_3P and $Ni_{12}P_5$ phases; and annealing at > 400 °C for 1 hour leads to the formation of Ni and Ni_3P phases. In contrast, annealing of EL Ni-Co-B alloy coating at 300 °C for 1 hour itself leads to the formation of Ni and Co_3B phases and further annealing up to 600 °C for 1 hour increases the crystallinity of the deposit. Thermomagnetic study of EL Ni-Co-P alloy

coating exhibits the Curie transition of nickel and non-stoichiometric Ni_3Co and Ni–Co based alloys whereas the Curie transition peaks corresponding to nickel and Co_3B are observed for EL Ni-Co-B alloy coating. EL Ni–Co–P and Ni-Co-B alloy coatings exhibit soft magnetic characteristics. The saturation magnetization, remanence and coercivity are found to increase with increase in cobalt content of these coatings.

4.5.2 Electroless Ni-W-P and Ni-W-B ternary alloy coatings

The formation of EL Ni-P and Ni-B binary and, EL Ni-W-P and Ni-W-B ternary alloy coatings and their characteristic properties are studied by Palaniappa /60/. The EL Ni-P and Ni-W-P coatings are prepared using acidic as well as alkaline hypophosphite-reduced EL plating baths whereas the EL Ni-B and Ni-W-B coatings are prepared using an alkaline DMAB-reduced EL plating bath. The alkaline hypophosphite-reduced EL plating bath with 20 g/l of sodium tungstate has resulted in coatings with maximum tungsten content (18 wt.%). Increase in sodium tungstate concentration beyond 20 g/l has no significant influence on the tungsten content of the coating. The increase in tungsten content of EL Ni-P and Ni-B coatings results in a reduction in the phosphorus and boron content, respectively and increases the crystallinity of these coatings. Alloying of tungsten in the EL Ni-P and Ni-B matrix increases the crystallization temperature of the resultant coatings. Heat treatment leads to crystallization of all deposits and heating at high temperatures leads to extensive growth in the size of the crystals /60-62/.

Alloying of tungsten in EL Ni-P as well as Ni-B matrix increases the hardness of the resultant coatings /62/. The extent of increase in hardness is a function of the tungsten content of these coating. Increase in heat treatment temperature increases the hardness of the coatings up to the grain coarsening limit in Ni-P and Ni-B binary alloy coatings whereas with alloying of tungsten in Ni-P as well as Ni-B matrix, the grain coarsening occurs at relatively higher temperatures compared to the binary alloy coatings (Fig. 16). Ni-B based binary and ternary alloy coatings is found to possess higher hardness compared to Ni-P based binary and ternary alloy coatings. EL Ni-W-P coatings prepared using the alkaline hypophosphite-reduced bath exhibit higher wear resistance compared to EL Ni-P coatings due to the higher amount of tungsten content in the coating which induces higher hardness by solid solution strengthening. EL Ni-B and Ni-W-B coating are

found to possess maximum hardness and exhibit maximum resistance to wear. EL Ni-B and Ni-W-B coatings possess lower frictional coefficient due to their unique cauliflower like structure which reduces the area of contact of the mating surfaces. Heat treatment further increases the hardness and wear resistance of the deposits up to 400°C for Ni-P and Ni-B binary alloy coatings and 500 °C for Ni-W-P and Ni-W-B ternary alloy deposits. Beyond this range, the tribological properties are found to deteriorate due to extensive growth in the crystal size.

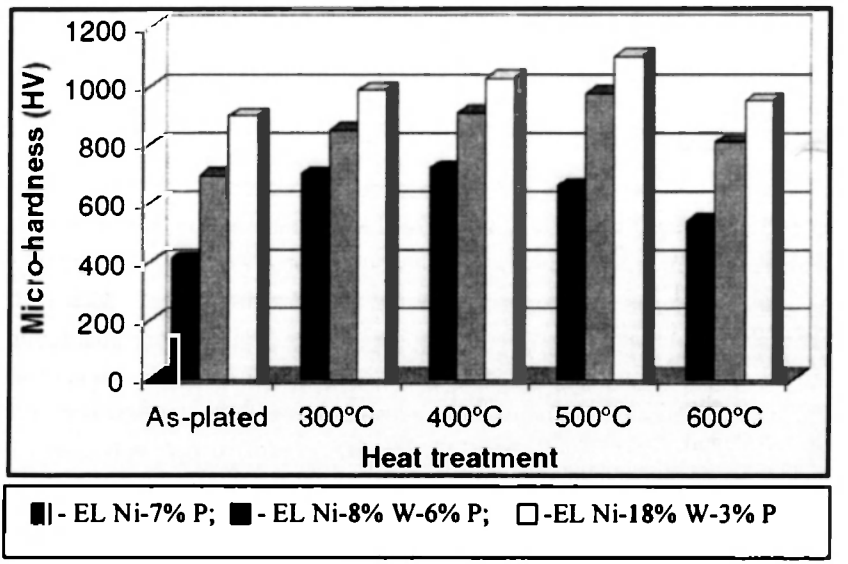

Fig. 16: Change in hardness as a function of heat-treatment temperature of EL Ni-P binary and Ni-W-P ternary alloy coatings obtained using an alkaline hypophosphite-reduced electroless plating bath (adapted from /60/)

Corrosion resistance of EL Ni-P, Ni-B, Ni-W-P and Ni-W-B coatings is found to be a function of the phosphorus/boron and tungsten content of the coating. EL Ni-B and Ni-W-B coatings provide relatively lower corrosion resistance compared to EL Ni-P and Ni-W-P coatings. In both Ni-P and Ni-B system, increase in tungsten content of the coating increases the corrosion resistance. Heat treatment of the coatings reduces their resistance to corrosion. All coatings in their as-plated condition are found to passivate in sulphuric acid media while heat treated coatings do not passivate. The

EL Ni-B coating exhibit better resistance to high temperature oxidation compared to EL Ni-P coating. Alloying of tungsten in Ni-P as well as Ni-B matrix increases the high temperature oxidation resistance of the ternary alloy coatings compared to their binary counterparts.

4.5.3 Electroless Ni-W-P, Ni-Cu-P ternary and Ni-W-Cu-P quaternary alloy coatings

Balaraju *et al.* /63-68/ have studied the formation of EL Ni-W-P, Ni-Cu-P ternary and Ni-W-Cu-P quaternary alloy coatings using alkaline hypophosphite-reduced citrate based plating baths in which nickel sulphate/nickel chloride/nickel sulphamate, sodium tungstate and copper sulphate are used as the source of nickel, tungsten and copper, respectively. There was observed to be no significant change in the grain size, hardness and corrosion resistance of EL Ni-Cu-P coatings obtained from sulphate and chloride based plating baths, except for the fact that coatings obtained from chloride based baths are relatively smoother and exhibit fewer nodules. Alloying of tungsten or copper in the EL Ni-P matrix causes a decrease in phosphorus content, increase in grain size and results in a more nodular and coarse morphology. Alloying of W in the Ni-P matrix increases the hardness and crystallization temperature. The activation energy for crystallization of EL Ni-P and Ni-W-P coatings are 229 and 289 kJ/mol, respectively. Alloying of copper in the EL Ni-P-W matrix has only a marginal influence on the composition of the coating, hardness and corrosion resistance. However, alloying of copper suppresses the coarse nodules and results in a smooth and nodule free coating.

4.5.4 Electroless Ni-W-P, Ni-Sn-P ternary and Ni-W-Sn-P quaternary alloy coatings

Balaraju *et al.* /69/ have studied the formation of EL Ni–Sn–P and Ni–W–P ternary and Ni–W–Sn–P quaternary alloy coatings using alkaline citrate-based baths and compared the characteristic properties of the ternary and quaternary alloy coatings with that of EL Ni–P binary alloy coatings. Alloying of Sn in the EL Ni-P matrix causes a slight decrease in the P content from 11.3 to 10.3 wt.% whereas alloying of W or both Sn and W in the EL Ni-P matrix causes a relatively large decrease in the P content; from 11.3 to 7.8 wt.% for alloying with W and from 11.3 to 6.4 wt.% for alloying with both Sn and W. The EL Ni-Sn-P and Ni-W-P ternary alloy coatings

exhibit a smooth nodular appearance, whereas a well-defined coarse nodular feature is observed for EL Ni-W-Sn-P quaternary alloy deposits. DSC thermogram of ternary Ni–Sn–P ternary alloy coating exhibits only a single exothermic peak, whereas higher peak transformation temperature and activation energies are observed for ternary Ni–W–P and quaternary Ni–W–Sn–P alloy coatings, suggesting an improvement in thermal stability following alloying with W or with both W and Sn.

4.6 Electroless Ni-P and Ni-B composite coatings

The idea of codepositing various second phase particles in EL nickel deposit and thereby taking advantage of its inherent uniformity, corrosion resistance and hardenability has led to the development of EL nickel composite coatings /70-72/. An essential advantage of preparing composite coatings by EL deposition compared to electro-codeposition is that the former allows accurate reproduction of the base geometry and eliminates the need for subsequent mechanical finishing. The EL composite coating is formed by the impingement and settling of particles on the surface of the work piece, and subsequent envelopment of these particles by the matrix material as it is deposited. There is no molecular bonding between particles and metal matrix. Several factors influence the incorporation of hard and soft particles in an EL Ni–P matrix including, particle size and shape, relative density of the particle, particle charge, inertness of the particle, the concentration of particles in the plating bath, the method and degree of agitation, the compatibility of the particle with the matrix, and the orientation of the part being plated.

4.6.1 Electroless Ni-P-Si_3N_4, Ni-P-CeO_2 and Ni-P-TiO_2 composite coatings

The formation of EL Ni-P-Si_3N_4, Ni-P-CeO_2 and Ni-P-TiO_2 using an acidic hypophosphite-reduced EL nickel bath and their characteristic properties are studied by Balaraju /73/. The level of incorporation of Si_3N_4, CeO_2 and TiO_2 particles in the Ni-P matrix increases with increase in their concentration in the bath up to 10 g/l, beyond which it attains saturation. The particles are uniformly distributed in the Ni-P matrix throughout its thickness (Fig. 17).

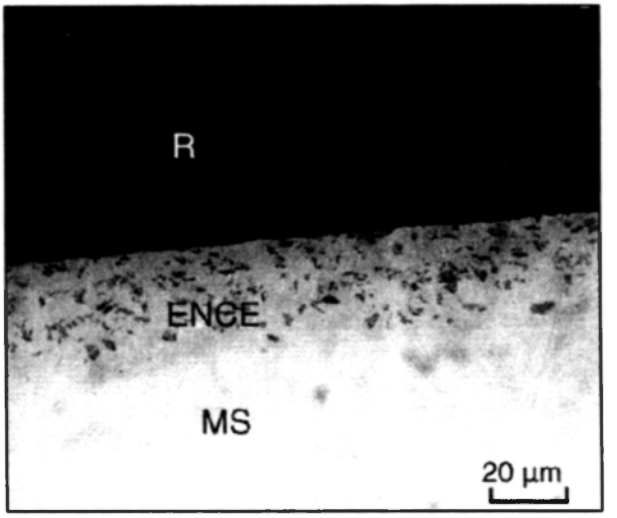

Fig. 17: Optical micrograph of the cross section of EL Ni–P–CeO_2 composite coating (Reprinted from *Materials Research Bulletin*, Vol. 41, J.N. Balaraju, T.S.N. Sankara Narayanan and S.K. Seshadri, Structure and phase transformation behaviour of electroless Ni–P composite coatings, pp. 847-860 (2006) with permission from Elsevier Science)

X-ray diffraction patterns of EL Ni P Si_3N_4, Ni P CeO_2 and Ni–P–TiO_2 composite coatings are very similar to that of plain EL Ni–P coating, both in as plated and heat-treated conditions. Selected area electron diffraction (SAED) patterns obtained on the Ni–P matrix of these composite coatings exhibit diffuse ring patterns resembling the one obtained for plain EL Ni–P coating. Phase transformation behaviour studied by differential scanning calorimetry (DSC) indicates that the variation in crystallization temperature and the energy evolved during crystallization of plain EL Ni–P coating and EL Ni–P–Si_3N_4, Ni–P–CeO_2 and Ni–P–TiO_2 composite coatings is not significant. These observations confirm that the Si_3N_4, CeO_2 and TiO_2 particles incorporated in the Ni-P matrix do not have any influence on structure and phase transformation behaviour of the resultant composite coatings /74/. The EL Ni-P-Si_3N_4, Ni-P-CeO_2 and Ni-P-TiO_2 composite coatings exhibit higher hardness, better resistance to wear, corrosion and high temperature oxidation, compared to plain Ni-P coating /73, 75/. Among the composite coatings, EL Ni-P-Si_3N_4 coating exhibits maximum hardness and

better resistance to wear, corrosion and high temperature oxidation, due to the higher level of incorporation of Si_3N_4 particles in the Ni-P matrix compared to CeO_2 and TiO_2.

4.6.2 Electroless Ni-P-Si_3N_4 composite coatings

Das *et al.* /76/ have studied the formation of EL Ni-P-Si_3N_4 composite coatings using an acidic hypophosphite-reduced EL plating bath and evaluated their corrosion and wear behaviour. The level of incorporation of Si_3N_4 particles in the EL Ni-6.5 wt.% P matrix increases with increase in bath loading, temperature and pH of the bath. The maximum incorporation obtained at a bath loading of 10 g/l is 4 wt.%. Further increase in concentration of the Si_3N_4 particles up to 20 g/l, however, results in a decrease in Si_3N_4 content of the coating. Uniform distribution of Si_3N_4 particles throughout the thickness of the EL Ni-P matrix is obtained at 2.9 wt.% whereas at higher levels of incorporation, clustering of Si_3N_4 particles is observed. The incorporation of Si_3N_4 particles (2.9 wt.%) in the EL Ni-P matrix did not have any influence on the structure and phase transformation behaviour. Incorporation of Si_3N_4 particles (2.9 wt.%) in the EL Ni-P matrix (4 μm thick) introduce more defects in the matrix in the form of increased porosity and provide easy access of the corroding media to the surface resulting in the loss of corrosion protection in pH 10 water. Tribological tests conducted on AISI 52100 ball-bearings and races coated with 4 μm thick EL Ni-6.5 wt.%P-2.9 wt.% Si_3N_4 composite coating in demineralized water at pH 10 using four-ball tester showed that the composite coating can last about 0.36 million load cycles or 9 years of life (25 years life corresponds to 1 million load cycle) in actual application.

4.6.3 Electroless Ni-B-Si_3N_4 composite coatings

The formation of EL Ni-B-Si_3N_4 composite coating and evaluation of its characteristic properties was studied by Krishnaveni /22/. The EL Ni-B-Si_3N_4 composite coating is prepared by dispersing the Si_3N_4 particles in an alkaline borohydride-reduced EL nickel plating bath. The level of incorporation of Si_3N_4 particles in the EL Ni-B matrix increases with increase in its concentration in the bath up to 10 g/L, beyond which it gets saturated. The maximum level of incorporation obtained at a bath loading of 10 g/l of Si_3N_4 particles is 2 wt.%. The EL Ni-B-Si_3N_4 composite coating contains 91.7 wt.% Ni; 6.0 wt.% B; 0.3 wt.% Tl; and 2 wt.% Si_3N_4 particles. The incorporation

of Si_3N_4 particles in the EL Ni-B matrix increases the surface roughness of the coatings. The average surface roughness (R_a) is of the order of 0.92 μm. The surface morphology of the coating reveals uniform distribution of Si_3N_4 particles in the EL Ni-B matrix. Incorporation of Si_3N_4 particles in the EL Ni-B matrix has a very little influence on the structure of EL Ni-B matrix. The grain size of the EL Ni-B-Si_3N_4 composite coatings is of the same order as that of EL Ni-B coatings; 2 to 3 nm in as-plated condition and 8 to 10 nm after heat-treatment at 450 °C for 1 hour.

The microhardness of as-plated EL Ni-B-Si_3N_4 composite coatings is 670 $HV_{0.1}$ and it increases to 946 $HV_{0.1}$ and 1012 $HV_{0.1}$, when the coating is heat-treated at 350 and 450 °C for 1 hour, respectively. The microhardness of EL Ni-B-Si_3N_4 composite coatings is relatively higher than that of EL Ni-B coatings, due to the combination strengthening of solid solution hardening of the matrix and dispersion hardening induced by particle incorporation. The wear resistance is higher for heat-treated EL Ni-B-Si_3N_4 composite coatings compared to those obtained in as-plated condition (Fig. 18)

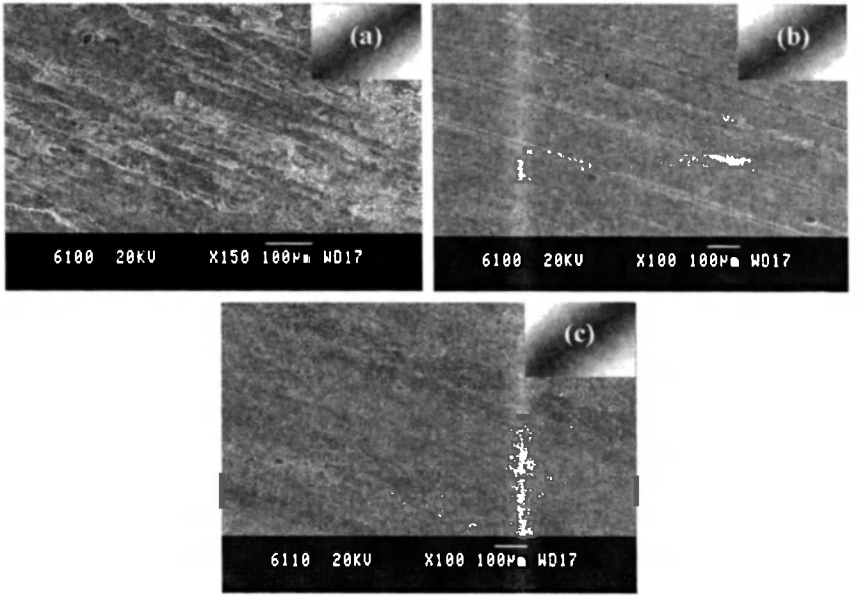

Fig. 18: Wear track pattern of EL Ni-B-Si_3N_4 composite coating (a) as-plated; (b) heat-treated at 350 °C for 1 hour; and (c) heat-treated at 450° C for 1 hour (Applied load: 40 N; Sliding distance: 2700 m) (adapted from /22/)

The wear resistance of EL Ni-B-Si_3N_4 composite coatings is relatively higher than that of EL Ni-B coatings, both in as-plated and heat-treated conditions, due to the double strengthening effect of the hard Si_3N_4 particles and precipitation strengthening of the Ni-B alloy matrix. The wear mechanism of EL Ni-B and EL Ni-B-Si_3N_4 composite coatings is similar - Adhesive wear appears to be the most likely mechanism during the wear process of EL Ni-B-Si_3N_4 composite coatings. Surface heterogeneity and columnar structure are primarily responsible for the observed corrosion behaviour of the EL Ni-B-Si_3N_4 composite coating in their as-plated condition. The corrosion resistance decreases further up on heat-treatment due to the crystallization of the coating, increase in the grain boundary region and formation of nickel boride phases. The corrosion resistance of EL Ni-B-Si_3N_4 composite coating is relatively higher than EL Ni-B coatings, both in as-plated and heat-treated conditions, due to the decrease in the effective metallic area prone to corrosion.

4.6.4 Electroless Ni-P-Al_2O_3 composite coatings

The influence of the particle size of alumina particles on the microstructure, hardness and corrosion resistance of EL Ni-P-Al_2O_3 composite coatings is studied by Balaraju *et al.* /77/. An acidic hypophosphite-reduced EL plating bath wherein the alumina particles are dispersed are used to prepare the EL Ni-P-Al_2O_3 composite coatings. The incorporation of Al_2O_3 particles has a marginal influence on the composition of the composite coatings whereas it does not influence the structure. Higher level of incorporation and uniform distribution are observed for Al_2O_3 particles with a particle size of 1 μm (8 wt.%) compared to those with a size of 0.3 μm (3.7 wt.%) and 50 nm (2.4 wt.%). Increasing the size of Al_2O_3 particles from 50 nm to 0.3 μm has reduced the nodularity of the coating whereas no nodules are seen in composite coatings prepared using 1 μm size Al_2O_3 particles. Only a marginal increase in hardness is observed for composite coatings compared to Ni–P coating in as-plated condition. However, the increase in hardness is found to be more after annealing the composite coatings at 400 °C for 1 hour. A marginal difference in corrosion resistance is observed for all the composite coatings. Composite coatings incorporate with 50 nm and 0.3 μm Al_2O_3 particles exhibit uniform corrosion whereas localized corrosion is observed in composite coatings incorporated with 1 μm Al_2O_3 particles.

4.6.5 Electroless Ni-P-diamond composite coatings

Reddy *et al.* /78/ have studied the formation of EL Ni–P–diamond composite coatings using an alkaline hypophosphite-reduced bath and evaluated their wear resistance in as-plated and heat-treated (230, 350 and 400 °C for 2 hour) conditions. The phosphorus content of the EL Ni-P matrix is varied by changing the concentration of hypophosphite in the bath. The diamond particles are in the size range of 3 to 6, 6 to12 and 20 to 40 μm and their incorporation in the EL Ni-P matrix having a thickness of 20 μm is studied. The EL Ni-P matrix with lower phosphorus content exhibit very little integrity with the diamond particles compared to the matrix with higher phosphorus content. EL Ni-P matrix with 9 to 10 wt.%. P performs marginally better. Irrespective of the phosphorus content of the EL Ni-P matrix, 20 to 40 μm diamond particles are less firmly held, suggesting that for better integrity between the particle and nickel matrix, there should be an optimum ratio between the coating thickness and the size of the particles. EL Ni–P–diamond composite coatings incorporated with finer diamond particles are found to be more wear resistant compared to those incorporated with coarse particles. The wear resistance of the EL Ni-P-diamond composite coatings also increases with increase of phosphorus content of the matrix. Heat-treatment of EL Ni-P-diamond composite coating increases their wear resistance, following the precipitation of the hard nickel phosphide phases.

Co-deposition of very fine particles of polycrystalline diamond particles in a nickel matrix can be carried out by both electro- and electroless deposition processes. Irrespective of the deposition process, the wear resistance of the Ni-diamond composite coatings will depend on how firmly the diamond particles are anchored in the matrix. Sheela and Pushpavanam /79/ have studied the formation of EL Ni-P diamond composite coatings from an acidic hypophosphite-reduced EL plating bath by sediment co-deposition process. Natural diamond powder (8 to 12 μm) in the concentration range of 2 to 10 g/l in the bath is used to prepare the EL Ni-P-diamond composite coatings. Using the sediment co-deposition method, it is possible to incorporate around 30 vol. % of diamond particles in the EL Ni-P matrix using a very low amount of diamond powders in suspension. The hardness of the EL Ni-P-diamond composite coating is similar to hard chromium coating.

4.6.6 *Electroless Ni-P and Ni-P-TiO_2 composite coating*

Nickel-based electrodes alloyed with non-metallic elements such as phosphorous have been developed for hydrogen evolution reaction (HER) due to their high electrocatalytic activity. Shibili *et al.* /80/ have studied the physicochemical and electrocatalytic properties of EL Ni–P coatings with varying P content in the range of 3 to 18 wt.%. EL Ni-P coating with 10 wt.% P, which consists of a mixture of amorphous and crystalline phases is found to offer high electrocatalytic activity for HER. The high surface roughness and presence of large number of electro-active sites in EL Ni-10 wt.% P coating facilitate maximum extent of hydrogen adsorption on its surface. The EL Ni-P-TiO_2 composite coating is prepared by dispersing nanosized TiO_2 powders (90 to 130 nm) in the EL plating bath. The reinforcement of TiO_2 particles in the EL Ni-P matrix further enhanced the roughness factor, the number of electro-active sites and hydrogen adsorption ability. The EL Ni-P-TiO_2 composite coating exhibit better electrocatalytic activity for HER compared to EL Ni-P coating.

4.6.7 *Electroless Ni-P-ZrO_2-Al_2O_3 composite coating*

Sharma *et al.* /81, 82/ have studied the formation of EL Ni-P-ZrO_2-Al_2O_3 composite coating on aluminium by in-situ co-precipitation and co-deposition method and evaluated their dry sliding wear behaviour in as-plated and heat-treated conditions. The EL Ni-P-ZrO_2-Al_2O_3 composite coating is prepared using an alkaline hypophosphite-reduced EL plating bath which contains aluminum chloride and zirconium oxychloride as the source of Al_2O_3 and ZrO_2 in the coating. The EL Ni-P-ZrO_2-Al_2O_3 composite coating is pore free and well-adherent on the aluminum substrate. Quantitative analysis of the EL Ni-P-ZrO_2-Al_2O_3 composite coating by EPMA reveals that the coating contains 9.5% P, 0.287% ZrO_2, 0.025% Al_2O_3 with Ni as the balance. Heat treatment of EL Ni-P-ZrO_2-Al_2O_3 composite coating at 400°C for 1 hour as well as at 250°C for 12 hour significantly increases the microhardness of the coatings. The wear rate of EL Ni-P-ZrO_2-Al_2O_3 composite coating is much lower compared to uncoated aluminum substrate. The wear rate of EL Ni-P-ZrO_2-Al_2O_3 composite coating heat-treated at 250 °C for 12 hour is less than those heat-treated at 400°C for 1 hour.

4.6.8 Electroless Ni-P-ferrite composite coatings

Agarwala /83/ have prepared EL Ni-P-ferrite composite coatings using nano-grained $BaZn_{2-y}Co_yFe_{16}O_{27}$ (Y = 0:0, 0.4, 0.8, 1.2, 1.6 and 2.0) powders as the second phase particles in an alkaline-hypophosphite reduced EL plating bath. The EL Ni-P-ferrite composite coatings exhibit microwave absorption property, which can be exploited for radar applications. The microwave absorption reaches a maximum level at 14.4 GHz. The extent of absorption increases with increase in concentration of nanograined $BaZn_{2-y}Co_yFe_{16}O_{27}$ powders in the bath. The microwave absorption is 4.0 and 6.2 dB for coatings obtained in the presence of 5 g/l and 10 g/l of ferrite powder, respectively.

4.7 Electroless plating of metallic and ceramic powders

4.7.1 Electroless nickel plating of Ti and Al powders for P/M processing

The feasibility of EL nickel plating of Ti and Al metal powders has been explored by Ramaseshan *et al.* /84/. The Ti (< 75 μm) and Al (< 45 μm) powders are mixed in the ratio of 80:20, pretreated using a nickel based electrolyte solution and coated using an alkaline hypophosphite-reduced EL nickel plating bath. The coating time is varied between 5 to 40 minutes. The coated powders can be used to prepare γ-TiAl based alloys, which can be subsequently used as a matrix material to prepare γ-TiAl alloy composite. The γ-TiAl alloy composite offers better oxidation resistance, toughness and wear resistance.

4.7.2 Electroless copper coating of Al-Si oxide powders

Copper coated ceramic powders find widespread application in electronics, aerospace, medical, oil and gas production, chemical production, etc. Rahul Sharma *et al.* /85/ have developed a method for EL copper plating of Al-Si oxide powders. The Al–Si oxide powder (size: 100 μm) is sensitized and activated by immersion in $SnCl_2$ (5 g/l) and $PdCl_2$ (0.01 g/l $PdCl_2$ + 0.1 ml/l HCl), respectively and subsequently coated with copper by EL plating technique. The temperature and pH of the plating bath influences the deposition rate as well as the color of the coating. The optimum combination of temperature and pH of the EL copper bath is 75 °C and 12.5, respectively, which attributes to the bright maroon color of the coating with increase in weight of 60%.

The color of the coated powder is changed from bright to darker shades after heat treatment. The EL copper coating is globular in nature. The EL copper coating is found to be uniform not only over the plane surfaces of the ceramic particles but also inside the porous regions of the particles. The nucleation of the coating process starts with globules in nano-size range, which then grows laterally to cover the whole surface with high uniformity. Subsequently, a vertical growth follows. Mechanical bonding created by the anchoring of globules inside the nano- and micro-sized pores (cauliflower structure), provides very good adherence over the surface of all the substrates coated with copper. The proposed new mechanism of EL copper coating over the surface is not only the chemical bonding but also mechanical bonding.

4.7.3 EL Ni-P coating on graphite powders

Electroless plating of metal on ceramic substrates requires the use of sensitization using $SnCl_2$ followed by activation using a mixture of $PdCl_2$ and HCl, prior to plating. Palaniappa *et al.* /86/ have developed an alternate method for EL nickel plating of graphite particles, which is different from the conventional sensitisation and activation treatments. The activation process is carried out by heating the graphite particles in muffle furnace at 380 °C for 1 hour in air. This treatment enables removal of any adsorbed gases from the surface of the graphite powders, resulting in a clean active surface, which enhances wettability of the powders in the aqueous solution for the metal-ion species. Using this treatment a uniform and continuous layer of nickel could be deposited on the surface of graphite particles by EL plating technique. The amount of nickel deposited does not vary much with increase in size of the graphite particles. However, a significant variation in the amount of nickel deposited is observed with an increase in bath loading following the increase in effective surface area of the graphite powders.

The effect of EL Ni-P coated graphite powders on the electrocatalytic oxidation of dextrose in 0.1 M KOH, in comparison with pure nickel powder, is evaluated by Veerababu *et al.* /87/. The BET surface area of pure Ni, activated graphite and EL Ni-P coated graphite powders are 10.4, 14.8 and 12.2 m^2/g, respectively. The surface area of EL Ni-P coated graphite powders is higher than that of pure Ni powders but lower than that of activated graphite powders. The catalytic ability of pure Ni and EL Ni–P coated graphite powders is evaluated using the electro-oxidation of dextrose (1.8×10^{-3} to 4.5×10^{-3} M) in 0.1 M KOH solution. EL Ni–P coated graphite

powders exhibit better catalytic activity for the electro-oxidation of dextrose compared to pure Ni powders. The electrocatalytic efficiency for the electro-oxidation of 4.5×10^{-3} M dextrose over Ni-P coated graphite powders is found to be approximately three times higher compared to pure Ni powder. The difference in performance is attributed to the graphite particles on which the Ni-P alloy is coated, which increases the surface area of the composite.

4.7.4 Electroless plating of YSZ powders

Solid oxide fuel cells (SOFC) are important as energy conversion systems due to their high efficiency, design modularity and environment friendly nature. Nickel-yttria stabilized zirconia (Ni-YSZ) cermet is widely used as an anode material for solid oxide fuel cells (SOFCs). The metallic conductivity of Ni-YSZ cermet (above percolation threshold) is achieved by the formation Ni-to-Ni chain within the cermet matrix. Pratihar *et al.* /88/ have explored the possibilities of utilizing EL plating technique to prepare a uniform nickel coating on the YSZ powder. Their study reveals that a uniform nickel coating on YSZ powder without any impurity phase can be obtained by EL plating technique. The EL nickel plated YSZ powders are found to be electrically conducting even in 'as-pressed' condition and the conductivity percolation threshold is as low as 10 to 20 vol.% of Ni, which is much lower than that of the conventional Ni-YSZ cermets (20 to 30 vol.% of Ni). The conductivity value of the Ni-YSZ cermet containing 20 vol.% of Ni, sintered at 1000°C, is as high as 450 S/cm. Pratihar *et al.* /88/ have suggested that Ni-YSZ cermets prepared by EL plating technique are well suited for SOFC anode applications compared to those prepared by conventional techniques.

The amount of Ni required to completely cover the YSZ surface depends on the size of the YSZ powders. By increasing the size of the YSZ powders, it is possible to decrease the amount of Ni required for complete coverage of the YSZ surface and to reduce its thermal expansion coefficient. However, a minimum concentration of nickel is also required to have sufficient electrical conductivity. In this perspective, Pratihar *et al.* /89/ have studied the EL nickel plating of YSZ powders having two different particle sizes, viz., powders with a d_{50} of 0.40 μm and 0.85 μm. The nickel content of the coated powders is varied from 7.23 to 64.99 wt.% in the Ni-YSZ cermet. Their study reveals that the electrical conductivity of Ni-YSZ cermet is strongly dependent on its nickel content. A sudden increase in conductivity is observed around 27.04 wt.% of nickel. For a fixed matrix density, the

conductivity is found to increase with increasing YSZ particle size. At a constant nickel loading the coating thickness increases with increasing YSZ particle size resulting in higher conductivity. The conductivity also increases significantly with decrease in matrix porosity due to better particle-to-particle contact between the nickel particles. Porous Ni-YSZ cermets are electronically conducting at Ni contents greater than 27.04 wt.% of total solids. Below 14.14 wt.% nickel the conductivity falls to that of the ionically conducting zirconia matrix. The conductivity percolation thresholds for these cermets are as low as 14.14 to 27.04 wt.% nickel. Large size YSZ particles are better suited for higher conductivity.

4.7.5 Microencapsulation of rare-earth alloy powders for Ni-MH batteries

The development of the Ni-MH battery has broadened the application of hydrogen storage alloys in the battery industry. Microencapsulation is a process of EL plating of the alloy powders, with a thin layer of Cu, Ni–P, Ni–B, Pd and Co. The microencapsulation of $ZrMn_{0.2}V_{0.2}Fe_{0.8}Ni_{0.8}$ alloy powder with Cu, Ni and Pd and the characteristics of the electrodes fabricated using these powders are studied by Parimala *et al.* /90/. The activation time taken for the electrodes prepared using the Cu, Ni and Pd microencapsulated $ZrMn_{0.2}V_{0.2}Fe_{0.8}Ni_{0.8}$ alloy powders to reach the maximum capacity is decreased considerably compared to those made with bare alloy powders. This is due to the increase in cell volume and the different catalytic effects of the Cu, Ni and Pd coatings on the hydrogen evolution reaction. The maximum discharge capacity is achieved for the Pd coated alloy (242 mA.h/g) whereas Ni and Cu coated alloys gave almost equal discharge capacity (214 mA.h/g and 211 mA.h/g for Ni and Cu coated alloy, respectively). The ability of the Pd coating to increase the hydriding/dehydriding reaction of the electrode in an alkaline solution offers it to yield a better performance than Cu and Ni coating.

5. CONCLUDING REMARKS

The recent developments in the areas of phosphate conversion coatings, electrodeposition and EL deposition are reviewed. Development of energy efficient and eco-friendly processes has been the main focus in the area of phosphate conversion coatings. Galvanic coupling of steel with metals that

are nobler than steel, seems to be a simple and effective means of accelerating low temperature phosphating process. Cathodic electrochemical treatment during phosphating offers numerous opportunities to prepare a variety of composite coatings using different combinations of metal ions in the solution, type of anode materials, current density and time. The porous nature of phosphate coatings obtained by anodic electrochemical treatment will be more suitable for tube and wire drawing operations.

Development of electro- and electroless deposited nanocrystalline coatings has received considerable attention in recent years. Studies on ED of nanocrystalline Ni, Ni-B, Ni-W, Ni-W-Fe, Cu-Ni coatings and ED of CoNiFe nanorods using AAO templates are quite interesting. The development of polyalloy, duplex, multilayer and graded and composite coatings ascertain the ability of electro- and electroless deposition processes to tailor made coatings with desirable characteristics. Replacement of lead acetate with thiourea as a stabilizer in EL plating bath is a viable option, the choice of thiourea as a substitute for lead acetate should be made only after a careful study. The possibility of utilizing EL Ni-P coatings for corrosion protection of reinforcement bars, EL Ni-P coating as an interlayer to improve the corrosion resistance of PVD hard coatings, blackened EL Ni-P coatings as high absorptance coating for space applications, development of low temperature bath for EL Ni-B coatings, EL Ni-P and Ni-B coatings for corrosion protection of Nd-Fe-B magnets, are some of the interesting developments. EL plating of metallic and ceramic powders, though well established, studies on thermal activation of graphite powders for EL plating, the utility of EL Ni-P coated graphite powders as an electrocatalyst, EL plating of Ti and Al powders for P/M processing, EL plating of YSZ powders for fuel cells applications and microencapsulation of rare-earth alloy powders for Ni-MH batteries, are worth mentioning.

In spite of the numerous developments, there are many issues that need better understanding and remain unexplored. The corrosion resistance of electrodeposited nanocrystalline coatings is a debatable issue. The increase in grain boundaries in nanocrystalline coatings is likely to increase the corrosion rate. However, there are instances where the nanocrystalline coatings offer better corrosion resistance. It is believed that nanocrystalline coatings offer better corrosion resistance in electrolyte solutions which promote passivation, whereas their corrosion resistance is decreased when the conditions does not promote passivation. It is important to ascertain under what conditions

nanocrystalline coatings will offer better corrosion resistance and, if not, how to improve it. This calls for a thorough study.

The corrosion resistance of electro- and electroless composite coatings is also a debatable issue. The improvement or impairment of corrosion resistance of ED and EL composite coatings depends on the chemical stability of the particle, structural state or microstructural feature of the coating, porosity or defect size of the coating, ability to prevent diffusion of chloride ions along the interface between the metal and the particle, the ability of the particle to prevent the corrosive pits from growing up, etc. A thorough understanding is required on this aspect and it warrants further study.

Thallium salts are being used as a stabilizer in borohydride-reduced EL nickel plating baths to prepare EL Ni-B coatings with high hardness, better wear resistance and moderate corrosion resistance. Although lead nitrate and mercaptobenzothiazole are good in stabilizing the bath, the plating rate is poor in these baths. The only choice to achieve better bath stability and higher deposition rate is the addition of thallium compounds as stabilizers. This is due to the ability of thallium ions, which not only stabilizes the plating bath but also increases the reduction efficiency of borohydride. However, thallium salts are toxic and this calls for the development of an alternative eco-friendly stabilizer without compromising on the deposition rate and the desirable characteristics of the coating.

In the coming years, energy efficiency and eco-friendliness of the process will assume significance in the development of surface treatment processes.

REFERENCES

1. T.S.N. Sankara Narayanan, *Rev. Adv. Mater. Sci.*, **9** (2005) 130-177
2. K. Ravichandran, Harihar Sivanandh, S. Ganesh, T. Hariharasudan and T.S.N. Sankara Narayanan, *Met. Finish.*, **98**(9) (2000) 48-54.
3. K. Ravichandran and T.S.N. Sankara Narayanan, *Trans. Inst. Met. Finish.*, **79**(4) (2001) 143-145.
4. A. Arthanareeswari, T.S.N. Sankara Narayanan, K. Ravichandran and S. Rajeswari, *Indian Surf. Finish.*, **1**(1) (2004) 80-88.
5. A. Arthanareeswari, Ph.D. Thesis, University of Madras, Chennai, 2006.

6. S. Jegannathan, T.S.N. Sankara Narayanan, K. Ravichandran and S. Rajeswari, *Surf. Coat. Technol.*, **200** (12-13) (2006) 4117-4126.
7. S. Jegannathan, T.S.N. Sankara Narayanan, K. Ravichandran and S. Rajeswari, *Electrochim. Acta*, **51**(2) (2005) 247-256.
8. T.S.N. Sankara Narayanan, S. Jegannathan and K. Ravichandran, *Prog. Org. Coat.*, **55** (2006) 355-362.
9. S. Jegannathan, Ph.D. Thesis, University of Madras, Chennai, 2005.
10. S. Jegannathan, T.S.N. Sankara Narayanan, K. Ravichandran and S. Rajeswari, *Prog. Org. Coat.*, **57** (2006) 392-399.
11. S. Jegannathan, T.S.N. Sankara Narayanan, K. Ravichandran and S. Rajeswari, *Surf. Coat. Technol.*, **200** (2006) 6014–6021.
12. S. Jegannathan, T.K. Arumugam, T.S.N. Sankara Narayanan, K. Ravichandran, *Prog. Org. Coat.* (2008) (in press) (doi:10.1016/j.porgcoat.2008.11.009)
13. S. Palraj, M. Selvaraj and P. Jayakrishnan, *Prog. Org. Coat.*, **54** (2005) 5-9.
14. T.K. Rout, N. Bandyopadhyay and T. Venugopalan, *Surf. Coat. Technol.*, **201**(3-4) (2006) 1022-1030.
15. T.K. Rout, H.K. Pradhan and T. Venugopalan, *Surf. Coat. Technol.*, **201**(6) (2006) 3496-3501.
16. R. Mishra and R. Balasubramaniam, *Corros. Sci.* **46** (2004) 3019-3029.
17. R. Mishra, B. Basu and R. Balasubramaniam, *Mater. Sci. Eng., A*, **373** (2004) 370-373.
18. V. Ganesh, D. Vijayaraghavan and V. Lakshminarayanan, *Appl. Surf. Sci.*, **240** (2005) 286-295.
19. K. Krishnaveni, T.S.N. Sankara Narayanan and S.K. Seshadri, *Indian Surf. Finish.*, **1**(1) (2004) 52-58.
20. K. Krishnaveni, T.S.N. Sankara Narayanan and S.K. Seshadri, *Trans. Indian Inst. Met.*, **56**(4) (2003) 341-346.
21. K. Krishnaveni, T.S.N. Sankara Narayanan and S.K. Seshadri, *Mater. Chem. Phys.*, **99** (2006) 300-308.
22. K. Krishnaveni, Ph.D. Thesis, University of Madras, Chennai, 2007.
23. L. Anicai, *Corr. Rev.*, **25**(5-6) (2007) 607-620.
24. K.R. Sriraman, S. Ganesh Sundara Raman and S.K. Seshadri, *Mater. Sci. Eng., A*, **418** (2006) 303-311.
25. N. Eliaz, T.M. Sridhar and E. Gileadi, *Electrochim. Acta*, **50** (2005) 2893-2904.

26. T.M. Sridhar, N. Eliaz and E. Gileadi, *Electrochem. Solid-State Lett.*, **8** (2005) C58-C61.
27. N. Eliaz and E. Gileadi, *Electrochem. Soc. Trans.*, **2** (2007) 337-349.
28. N. Eliaz and E. Gileadi, "Induced Codeposition of Alloys of Tungsten, Molybdenum and Rhenium with Transition Metals," Chapter 4, in *Modern Aspects of Electrochemistry*, Vol. 42, C.G. Vayenas, R.E. White and M.E. Gamboa-Aldeco (Eds.), Springer, New York (2008) 191-301.
29. K.R. Sriraman, S. Ganesh Sundara Raman and S.K. Seshadri, *Mater. Sci. Eng., A*, **460–461** (2007) 39-45.
30. K.R. Sriraman, S. Ganesh Sundara Raman and S.K. Seshadri, *Mater. Sci. Technol.*, **22**(1) (2006) 14-20.
31. I. Baskaran, Ph.D. Thesis, University of Madras, Chennai, 2007.
32. I. Baskaran, T.S.N. Sankara Narayanan and A. Stephen, *Mater. Lett.*, **60**(16) (2006) 1990-1995.
33. S.K. Ghosh, G.K. Dey, R.O. Dusane and A.K. Grover, *J. Alloys Compd.*, **426** (2006) 235-243.
34. S.K. Ghosh, P.K. Limaye, S. Bhattacharya, N.L. Soni and A.K. Grover, *Surf. Coat. Technol.*, **201** (2007) 7441-7448.
35. V. Thangaraj, N. Eliaz and A.C. Hegde, *J. Appl. Electrochem.*, (in press) (DOI 10.1007/s10800-008-9677-1).
36. C. S. Ramesh and S. K. Seshadri, Wear, **255**(7-12) (2003) 893-902.
37. K. Krishnaveni, T.S.N. Sankara Narayanan and S.K. Seshadri, *J. Alloys Compd.*, **466** (2008) 412-420.
38. K. Krishnaveni, T.S.N. Sankara Narayanan and S.K. Seshadri, *J. Mater. Sci.* **44** (2009) 433-440.
39. S.T. Aruna, C.N. Bindu, V. Ezhil Selvi, V.K. William Grips and K.S. Rajam, *Surf. Coat. Technol.*, **200**(24) (2006) 6871-6880.
40. M. Surender, R. Balasubramaniam and B. Basu, *Surf. Coat. Technol.*, **187**(1) (2004) 93-97.
41. M. Surender, B. Basu and R. Balasubramaniam, *Tribology Int.*, **37**(9) (2004) 743-749.
42. Malathy Pushpavanam, H. Manikandan and K. Ramanathan, *Surf. Coat. Technol.*, **201**(14) (2007) 6372-6379.
43. Meenu Srivastava, V.K. William Grips and K.S. Rajam, *Appl. Surf. Sci.*, **253** (2007) 3814-3824.

44. B.M. Praveen, T.V. Venkatesha, Y. Arthoba Naik and K. Prashantha, *Surf. Coat. Technol.*, **201**(12) (2007) 5836-5842.
45. V.B. Singh and Pinky Pandey, *Surf. Coat. Technol.*, **200** (2006) 4511-4514.
46. S.M.A. Shibli, K.S. Beenakumari and N.D. Suma, *Biosens. Bioelectron.*, **22** (2006) 633–638.
47. I. Baskaran, T.S.N. Sankara Narayanan and A. Stephen, *Mater. Chem. Phys.* **99**(1) (2006) 117-126.
48. D.D.N. Singh and Rita Ghosh, *Surf. Coat. Technol.*, **201**(1-2) (2006) 90-101.
49. M.A. Sanchez, L.A. Parra, O.A. Perez, and O. de Rincon, *Corr. Rev.*, **19**(2) (2001) 105-118.
50. V.K. William Grips, V. Ezhil Selvi, Harish C. Barshilia and K.S. Rajam, *Electrochim. Acta*, **51**(17) (2006) 3461-3468.
51. V. Saxena, R. Uma Rani and A.K. Sharma, *Surf. Coat. Technol.*, **201**(3-4) (2006) 855-862.
52. T.S.N. Sankara Narayanan and S.K. Seshadri, *J. Alloys Compd.*, **165** (2004) 197-205.
53. K. Krishnaveni, T.S.N. Sankara Narayanan and S.K. Seshadri, *Surf. Coat. Technol.*, **190** (2005) 115-121.
54. I. Baskaran, R. Sakthikumar, T.S.N. Sankara Narayanan and A. Stephen, *Surf. Coat. Technol.*, **200**(24) (2006) 6888-6894.
55. I. Baskaran, T.S.N. Sankara Narayanan, A. Stephen, S. Pandian and V. Chandrasekaran, Private communications.
56. T.S.N. Sankara Narayanan, K. Krishnaveni and S.K. Seshadri, *Mater. Chem. Phys.*, **82**(3) (2003) 771-779.
57. T.S.N. Sankara Narayanan, I. Baskaran, K. Krishanaveni and S. Parthiban, *Surf. Coat. Technol.*, **200**(11) (2006) 3438-3445.
58. T.S.N. Sankara Narayanan, A. Stephan and S. Selvakumar, *Surf. Coat. Technol.*, **172** (2003) 298-307.
59. T.S.N. Sankara Narayanan, A. Stephen and S. Guruskanthan, *Surf. Coat. Technol.*, **179**(1) (2004) 56-62.
60. M. Palaniappa, Ph.D. Thesis, Indian Institute of Technology Madras, Chennai, 2005.
61. M. Palaniappa and S.K. Seshadri, *Mater. Sci. Eng., A*, **460-461** (2007) 638-644.

62. M. Palaniappa and S.K. Seshadri, *J. Mater. Sci.*, **42**(16) (2007) 6600-6606.
63. J.N. Balaraju, C. Anandan and K.S. Rajam, *Appl. Surf. Sci.*, **250**(1-4) (2005) 88-97.
64. J.N. Balaraju and K.S. Rajam, *Surf. Coat. Technol.*, **195** (2-3) (2005) 154-161.
65. J.N. Balaraju, V. Ezhil Selvi, V.K. William Grips and K.S. Rajam, *Electrochim. Acta*, **52**(3) (2006) 1064-1074.
66. J.N. Balaraju, C. Anandan and K.S. Rajam, *Surf. Coat. Technol.*, **200**(12-13) (2006) 3675-3681.
67. J.N. Balaraju, S. Millath Jahan, C. Anandan and K.S. Rajam, *Surf. Coat. Technol.*, **200**(16-17) (2006) 4885-4890.
68. J.N. Balaraju, S. Millath Jahan and K.S. Rajam, *Surf. Coat. Technol.*, **201**(3-4) (2006) 507-512.
69. J.N. Balaraju, S. Millath Jahan, Anjana Jain and K.S. Rajam, *J. Alloys Compd.*, **436**(1-2) (2007) 319-327.
70. J.N. Balaraju, T.S.N. Sankara Narayanan and S.K. Seshadri, *J. Appl. Electrochem.*, **33** (2003) 807-816.
71. R.C. Agarwala and Vijaya Agarwala, *Sadhana*, **28**(3-4) (2003) 475-493.
72. R.C. Agarwala, Vijaya Agarwala and Rahul Sharma, *Synth. React. Inorg. Met.-Org. Nano-Met. Chem.*, **36**(6) (2006) 493-515.
73. J.N. Balaraju, Ph.D. Thesis, Indian Institute of Technology Madras, Chennai, 2000.
74. J.N. Balaraju, T.S.N. Sankara Narayanan and S.K. Seshadri, *Mater. Res. Bull.*, **41** (2006) 847-860.
75. J.N. Balaraju, T.S.N. Sankara Narayanan and S.K. Seshadri, *J. Solid State Electrochem.*, **5**(5) (2001) 334-338.
76. C.M. Das, P.K. Limaye, A.K. Grover and A.K. Suri, *J. Alloys Compd.*, **436**(1-2) (2007) 328-334.
77. J.N. Balaraju, Kalavati and K.S. Rajam, *Surf. Coat. Technol.*, **200** (12-13) (2006) 3933-3941.
78. V. V. N. Reddy, B. Ramamoorthy and P. Kesavan Nair, *Wear*, **239**(1) (2000) 111-116.
79. G. Sheela and M. Pushpavanam, *Met. Finish.*, **100**(1) (2002) 45-47.
80. S.M.A. Shibli and V.S. Dilimon, *Int. J. Hydrogen Energy*, **32**(12) (2007) 1694-1700.

81. S.B. Sharma, R.C. Agarwala, V. Agarwala and S. Ray, *J. Mater. Manuf. Process*, **17**(5) (2002) 637-649.
82. S.B. Sharma, R.C. Agarwala V. Agarwala and K.G. Satyanarayana, *Metall. Mater. Trans. B*, **36B**(2) (2005) 23-31.
83. R.C. Agarwala, *PRAMANA*, **65**(5) (2005) 959-965.
84. R. Ramaseshan, S. K. Seshadri and N. G. Nair, *Scripta Mater.*, **45**(2) (2001) 183-189.
85. Rahul Sharma, R.C. Agarwala and V. Agarwala, *Appl. Surf. Sci.*, **252**(24) (2006) 8487-8493.
86. M. Palaniappa, G. Veera Babu and K. Balasubramanian, *Mater. Sci. Eng., A*, **471**(1-2) (2007) 165-168.
87. G. Veera Babu, M. Palaniappa, M. Jayalakshmi and K. Balasubramanian, *Solid State Electrochem.*, **11**(12) (2007) 1705-1712.
88. S.K. Pratihar, A. Das Sharma, R. N. Basu and H. S. Maiti, *J. Power Sources*, **129**(2) (2004) 138-142.
89. S.K. Pratihar, A. Das Sharma and H.S. Maiti, *Mater. Chem. Phys.*, **96**(2-3) (2006) 388-395.
90. R. Parimala, M. V. Ananth, S. Ramaprabhu and M. Raju, *Int. J. Hydrogen Energy*, **29**(5) (2004) 509-513.